

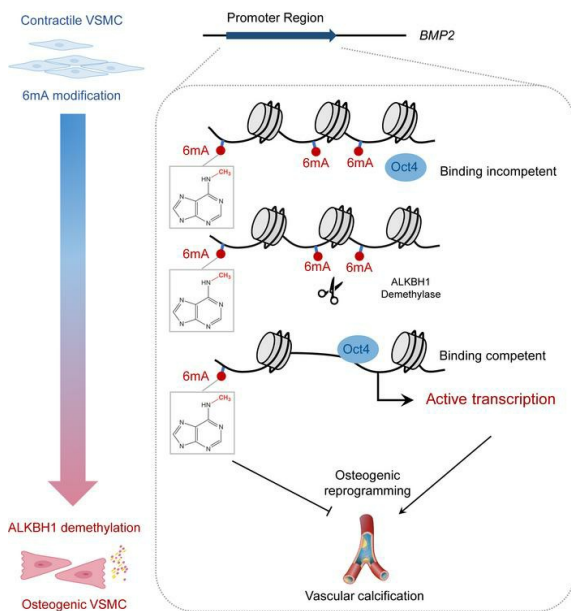
# ALKBH1-demethylated DNA N<sup>6</sup>-methyladenine modification triggers vascular calcification via osteogenic reprogramming in chronic kidney disease

Liu Ouyang, Xiaoyan Su, Wenxin Li, Liangqiu Tang, Mengbi Zhang, Yongjun Zhu, Changming Xie, Puhua Zhang, Jie Chen, Hui Huang

*J Clin Invest.* 2021. <https://doi.org/10.1172/JCI146985>.

Research In-Press Preview Cardiology Vascular biology

## Graphical abstract



Find the latest version:

<https://jci.me/146985/pdf>



1 **ALKBH1-demethylated DNA N<sup>6</sup>-methyladenine modification triggers vascular**  
2 **calcification via osteogenic reprogramming in chronic kidney disease**

3

4 **Liu Ouyang,<sup>1,2</sup> Xiaoyan Su,<sup>3</sup> Wenxin Li,<sup>2</sup> Liangqiu Tang,<sup>4</sup> Mengbi Zhang,<sup>3</sup> Yongjun**  
5 **Zhu,<sup>2</sup> Changming Xie,<sup>1,2</sup> Puhua Zhang,<sup>5</sup> Jie Chen,<sup>6</sup> Hui Huang<sup>1,2</sup>**

6

7 <sup>1</sup>Department of Cardiology, Sun Yat-sen Memorial Hospital, Guangzhou, China

8 <sup>2</sup>Department of Cardiology, the Eighth Affiliated Hospital of Sun Yat-sen University,  
9 Shenzhen, China

10 <sup>3</sup>Department of Nephropathy, Tungwah Hospital of Sun Yat-Sen University, Dongguan,  
11 China

12 <sup>4</sup>Department of Cardiology, Yuebei People's Hospital, Shantou University Medical  
13 College, Shaoguan, China

14 <sup>5</sup>Department of Nephrology, the First Affiliated Hospital of Sun Yat-sen University,  
15 Guangzhou, China

16 <sup>6</sup>Department of Radiation Oncology, Sun Yat-sen Memorial Hospital, Sun Yat-sen  
17 University, Guangzhou, China

18

19 **Address correspondence to:** Hui Huang, Department of Cardiology, the Eighth  
20 Affiliated Hospital of Sun Yat-sen University, Shennan Middle Rd, Shenzhen, China.

21 Email: huangh8@mail.sysu.edu.cn

22 **Authorship note:** LO, XS, WL, and LT are co-first authors.

23 **Conflicts of interest:** The authors have declared that no conflict of interest exists.

26 **Abstract**

27 Vascular calcification (VC) predicts cardiovascular morbidity and mortality in chronic  
28 kidney disease (CKD). To date, the underlying mechanisms remain unclear. We  
29 detected leukocyte DNA N<sup>6</sup>-methyladenine (6mA) levels in CKD patients with or without  
30 aortic arch calcification. We used arteries from CKD mice infected with vascular smooth  
31 muscle cells (VSMCs)-targeted adeno-associated virus encoding alkB homolog 1  
32 (*Alkbh1*) gene or *Alkbh1* shRNA to evaluate features of calcification. We identified that  
33 leukocyte 6mA levels were significantly reduced as the severity of VC increased in CKD  
34 patients. Decreased 6mA demethylation resulted from the upregulation of ALKBH1.  
35 Here, ALKBH1 overexpression aggravated, whereas its depletion blunted VC  
36 progression and osteogenic reprogramming in vivo and in vitro. Mechanistically,  
37 ALKBH1-demethylated DNA 6mA modification could facilitate the binding of octamer-  
38 binding transcription factor 4 (Oct4) to bone morphogenetic protein 2 (*BMP2*) promoter  
39 and activate *BMP2* transcription. This resulted in osteogenic reprogramming of VSMCs  
40 and subsequent VC progression. Either BMP2 or Oct4 depletion alleviated the pro-  
41 calcifying effects of ALKBH1. This suggests targeting ALKBH1 might be a therapeutic  
42 method to reduce the burden of VC in CKD.

44 **Introduction**

45 The leading cause of death in patients with chronic kidney disease (CKD) has been  
46 traced to cardiovascular complications (1). Medial vascular calcification (VC) is  
47 prevalent in CKD and contributes to subsequent cardiovascular morbidity and mortality  
48 (2). VC progressively increases with advanced stages of CKD and is linked with  
49 hyperphosphatemia (3). Hyperphosphatemia results in ectopic deposition of calcium-  
50 phosphate crystals in the vasculature. Thus, demonstrating that phosphate is a pivotal  
51 contributor to VC development. VC results in vessel wall stiffening and impaired elastic  
52 recoil (4). Consequently, the hemodynamic instability increases cardiac afterload and  
53 results in irreversible outcomes (5).

54 Multiple regions of the aorta are prone to calcification during CKD. Indeed, the aortic  
55 arch is more prone to calcification throughout the entire aorta at the early stage. Aortic  
56 arch calcification can easily be detected via chest computed tomography, which  
57 accurately represents the magnitude of VC (6). Aortic arch calcification is a prognostic  
58 indicator of worse cardiovascular outcomes (7). Various strategies have been devised to  
59 slow the progression of this burgeoning health concern. However, no substantial early  
60 diagnosis and practical pharmacological approach have been proved to retard VC.

61 Vascular smooth muscle cells (VSMCs) within the artery undergo osteogenic  
62 reprogramming to potentiate VC. This active process is recognized as similar to  
63 physiologic bone mineralization (8). Hyperphosphatemia drives VSMCs to convert from  
64 the contractile phenotype to the osteogenic phenotype, which is characterized by loss of  
65 VSMCs markers (smooth muscle 22 alpha [SM22 $\alpha$ ], alpha-smooth muscle actin [ $\alpha$ -SMA]

66 and Calponin1), accompanied with increased expression of osteogenic markers  
67 (osteopontin [OPN], osteocalcin [OCN] and Collagen I) (9). The bone morphogenetic  
68 proteins (BMPs) are members of the transforming growth factor beta family that  
69 engaged in embryogenesis, organogenesis, and osteoblast differentiation (10). Bone  
70 morphogenetic protein 2 (BMP2), a member of the BMPs family, is a potent osteogenic  
71 protein, which has been shown to promote VSMCs osteogenic reprogramming and VC.  
72 BMP2 accomplishes this by elevating the expression of runt-related transcription factor  
73 2 (RUNX2), the decisive transcription factor for bone formation (11).

74 Currently, there is limited understanding of how and why osteogenic reprogramming  
75 occurs. Epigenetic alterations to DNA methylation (12), histone modification (13), and  
76 microRNA have emerged as critical regulators of this process (14). DNA methylation  
77 abnormalities have been well described in CKD patients (12). Previous studies  
78 substantiated that elevated phosphate environment increased DNA methyltransferase  
79 activity and methylation of transgelin (TAGLN) promoter region. Thus, leading to  
80 decreased expression of SM22 $\alpha$  and a consequent increase in VC (15).

81 Recent developments in deep sequencing technology allowed the detection of a novel  
82 DNA adenine methylation (N<sup>6</sup>-methyladenine [6mA]) in the human genome (16). This  
83 modification is mediated by the methyltransferase N<sup>6</sup> adenine-specific DNA  
84 methyltransferase 1 (N6AMT1) and demethylase alkB homolog 1 (ALKBH1) (17).  
85 Several studies revealed that there is a robust relationship between ALKBH1-  
86 demethylated DNA 6mA modification and cardiovascular diseases, such as  
87 hypertension and atherosclerosis (18, 19). As previously reported, ALKBH1-mediated  
88 6mA demethylation is required for the osteogenic differentiation of human mesenchymal

89 stem cells during bone metabolism (20). However, the role of 6mA in VC has not been  
90 explored.

91 Considering the overlapping bone-vascular axis in VC, it is tempting to postulate that  
92 ALKBH1 may have a regulatory effect on the progression of VC. Therefore, this study  
93 was conducted to elucidate the role of ALKBH1-demethylated DNA 6mA modification in  
94 hyperphosphatemia-induced VC during CKD. We aim to provide new insights into early  
95 diagnosis and potential targets for therapeutic medication towards VC in CKD.

96

97 **Results**

98 *Reduced leukocyte DNA 6mA is correlated with the severity of vascular calcification in*  
99 *clinical.* CKD-induced hyperphosphatemia can elicit multiple alterations in cellular  
100 epigenetic regulation (21, 22). Leukocyte DNA 6mA levels were evaluated in CKD  
101 patients, with or without aortic arch calcification, to elucidate modification alterations  
102 during VC. The CKD patient characteristics in the Non-VC and VC group were shown in  
103 Table 1. To bolster confidence in the CKD cohort, we introduced the soluble urokinase  
104 plasminogen activator receptor (suPAR), which was proved as a practical and strong  
105 clinical indicator for renal disease (23-27). The plasma phosphate levels of CKD  
106 patients showed mild difference between two groups. This frustrating result may be  
107 accounted by the therapeutic controlling of hyperphosphatemia in recruited CKD  
108 patients. 32% CKD patients in Non-VC group accepted maintenance dialysis, and the  
109 percentage in VC group is 68% (Data not shown). The chest computed tomographic  
110 scan of CKD patients delineated the dense patchy calcification present in the wall of the  
111 aortic arch (Figure 1). Compared with non-calcification controls, 6mA levels were  
112 significantly reduced in CKD patients with calcification by approximately 49.6% (mean  
113  $0.0373 \pm 0.01\%$  vs.  $0.0188 \pm 0.007\%$ ) (Figure 2A). Next, we quantified aortic arch  
114 calcification in CKD patients by area and volume, which were presented as Agatston  
115 score and Volume score, respectively. As the severity of VC increased, 6mA levels  
116 progressively decreased. Individuals exhibiting the largest or thickest calcified lesions  
117 had the lowest 6mA levels (Figure 2, B and C). A negative correlation was observed  
118 between the DNA 6mA level and the calcification score in CKD patients with VC ( $R^2 =$   
119 0.4568 and  $R^2 = 0.4637$ , Pearson's correlation coefficient analysis) (Figure 2D,

120 Supplemental Figure 1A). Taken together, these data demonstrated that leukocyte 6mA  
121 levels are associated with VC progression in clinical.

122

123 *ALKBH1 is upregulated during vascular calcification.* The mRNA expression of *ALKBH1*,  
124 the 6mA demethylase was significantly elevated in CKD patients with VC, and *N6AMT1*,  
125 the 6mA methyltransferase was slightly decreased. Thus, alteration to the 6mA profile in  
126 leukocytes is mainly due to *ALKBH1* (Figure 2E). Interestingly, leukocyte *ALKBH1*  
127 mRNA expression was increased as VC progressed (Figure 2, F and G) and positively  
128 associated with the calcification score of CKD patients with VC (Figure 2H,  
129 Supplemental Figure 1B). Next, *ALKBH1*, *N6AMT1*, and 6mA were detected in radial  
130 artery specimens from CKD patients who underwent arterial-venous fistular surgery with  
131 diagnosed aortic arch calcification. Compared to normal controls, CKD specimens  
132 exhibited increased expression of *ALKBH1* and decreased 6mA modification (Figure 2,  
133 I-K). In addition, the CKD patients with VC showed advanced age according to the basal  
134 clinical characteristics of CKD patients (Table 1). However, 6mA levels were barely  
135 related to age in CKD patients with the presence or absence of VC (Supplemental  
136 Figure 1C).

137 To further verify the observations of 6mA levels in vivo, two mice models were utilized.  
138 The diet-induced CKD model is generated by feeding mice with 0.2% adenine diet for 8  
139 weeks. Surgery-promoted CKD model is conducted by performing 5/6 nephrectomy on  
140 mice. The plasma phosphorus, suPAR, blood urea nitrogen, and creatinine were  
141 elevated in both models (Supplemental Table 1-3). The renal histological staining of  
142 those mice showed similar increased inflammatory cells infiltration, tubule lumen

143 expansion, tubular vacuoles, interstitial fibrosis and mineral deposition in renal  
144 glomerulus, tubules and small vessels (Supplemental Figure 2 and 3). In addition, there  
145 is increased medial arterial calcification with a remarkable elevation of plasma alkaline  
146 phosphatase (ALP) (Supplemental Table 1-3). Therefore, VC is successfully induced in  
147 the CKD mice models. Consistent with the clinical observations in CKD patients with VC,  
148 leukocyte DNA 6mA level was decreased compared to controls (Figure 3A,  
149 Supplemental Figure 4A). Consistently, the calcification lesion size in the medial arterial  
150 layer of CKD mice had a negative correlation with lower leukocyte 6mA level (Figure 3,  
151 B and C, Supplemental Figure 4B). In addition, the mRNA expression of *Alkbh1* was  
152 significantly upregulated but not *N6amt1* in murine leukocytes (Figure 3D).  
153 Immunohistochemistry staining (Figure 3E, Supplemental Figure 4, C and D) and  
154 western blot analysis (Figure 3F, Supplemental Figure 4E) demonstrated elevated  
155 levels of ALKBH1 in aortic smooth muscle layers of CKD mice, and 6mA levels were  
156 markedly decreased. In comparison, N6AMT1 showed no alteration in expression. Of  
157 note, the enhanced ALKBH1 expression in the smooth muscle layer was inversely  
158 correlated to reduced leukocyte 6mA level (Supplemental Figure 5), suggesting the  
159 corresponding systematic change of 6mA modification in vivo. These observations were  
160 verified by ex vivo mice aortic rings cultured in osteogenic medium, which showed  
161 similar trends as the elevated ALKBH1 expression and corresponding decreased 6mA  
162 levels (Figure 3, G-I). Taken together, these data suggest that the ALKBH1 is  
163 upregulated in leukocyte and VSMCs during VC.

165 *Depletion of ALKBH1 alleviates vascular calcification.* ALKBH1 can be upregulated  
166 during VC, so it is interesting to address whether ALKBH1 depletion might attenuate the  
167 VC progression. Most of the global *Alkbh1* knockout mice died during the embryonic  
168 stage, and survivors exhibit developmental tissue defects (28). To elucidate ALKBH1  
169 function, we utilized the adeno-associated virus (AAV) infection as a genomic  
170 manipulation model. AAV carrying scrambled shRNA or *Alkbh1* shRNA (sh-ALKBH1)  
171 were inoculated via tail vein into two CKD mice models. Depletion of ALKBH1 in the  
172 aorta was confirmed via western blot analysis (Figure 4A). Knockdown of ALKBH1  
173 strikingly suppressed the calcium deposition and mineralization of the aorta compared  
174 to the scrambled controls (Figure 4, B-D, Supplemental Figure 6), along with the plasma  
175 ALP (Supplemental Table 1 and 3). To further confirm the *in vivo* results, we cultured  
176 primary murine VSMCs in an osteogenic medium for 2 weeks with sh-Scr or sh-  
177 ALKBH1. ALKBH1 knockdown cohorts exhibited significantly decreased calcium nodule  
178 formation as demonstrated by alizarin red staining (Figure 4E) and reduced calcium  
179 deposition, and the corresponding decreased ALP activity (Figure 4, F and G).  
180 Collectively, these results suggest that deficiency of ALKBH1 inhibits VC.

181

182 *Overexpression of ALKBH1 enhances vascular calcification.* To evaluate whether  
183 ALKBH1 could aggravate VC progression, we established an overexpression model by  
184 injecting AAV-Vector or AAV-ALKBH1 to CKD mice induced by adenine diet or operation.  
185 The efficiency of transfection was verified, as indicated in Figure 4H. As expected, AAV-  
186 ALKBH1 significantly increase *in vivo* calcification, as determined by von Kossa staining,  
187 calcium assay (Figure 4, I-K, Supplemental Figure 6), and quantification of plasma ALP

188 activity (Supplemental Table 2 and 3). In vitro results showed that AAV-Vector infection  
189 did not alter the calcium deposition in cultured murine VSMCs. In contrast, ALKBH1  
190 overexpression greatly exacerbated calcification progression (Figure 4, L-N), further  
191 suggesting that ALKBH1 promotes VC. The blood pressure of CKD patients showed  
192 difference between Non-VC and VC group (Table 1). In addition, ALKBH1 was  
193 associated with hypertension (19). However, we found systolic blood pressure, diastolic  
194 blood pressure, and other parameters including blood glucose, cholesterol, and  
195 triglyceride were not affected by ALKBH1 deficiency or overexpression in vivo  
196 (Supplemental Table 1-3, Supplemental Figure 7).

197

198 *ALKBH1 regulates osteogenic reprogramming of VSMCs.* We next determined whether  
199 ALKBH1 could regulate the osteogenic reprogramming of VSMCs in vitro and in vivo.  
200 High inorganic phosphate (Pi) condition successfully induces VSMCs osteogenic  
201 reprogramming (Figure 5A). Deletion (Figure 5, B and C) or overexpression (Figure 5, D  
202 and E) of *Alkbh1* in calcified mice primary VSMCs were confirmed by mRNA analysis  
203 and 6mA quantification. ALKBH1 deficiency dramatically suppressed the expression of  
204 osteogenic genes OPN, OCN, and Collagen I, and conversely increased expression of  
205 the contractile genes SM22 $\alpha$ ,  $\alpha$ -SMA, and Calponin1 (Figure 5F). In contrast, the levels  
206 of osteogenic markers were upregulated while the contractile makers were decreased  
207 as a result of the overexpression of ALKBH1 (Figure 5G). The aortas from 5/6-  
208 nephrectomy-induced CKD mice further confirmed that OCN and SM22 $\alpha$  expression  
209 were regulated by ALKBH1 (Supplemental Figure 8). Moreover, in HASMCs, ALKBH1  
210 deficiency could attenuate the osteogenic reprogramming together with the calcium

211 deposition (Supplemental Figure 9). Thus, these data show that ALKBH1 elevation  
212 promotes osteogenic reprogramming of VSMCs during calcification.

213

214 *BMP2 mediates ALKBH1-regulated VSMCs osteogenic reprogramming.* We detected  
215 transcription factors and signaling pathways that were vital during osteogenic  
216 reprogramming. ALKBH1 depletion altered BMP2 and RUNX2 expression but not SRY-  
217 box transcription factor 9 (SOX9) and distal-Less homeobox 5 (DLX5) (Figure 6A,  
218 Supplemental Figure 10). Immunofluorescence staining further confirmed that ALKBH1  
219 depletion suppressed BMP2 in aortas from CKD mice, along with reciprocal changes in  
220  $\alpha$ -SMA (Figure 6, B and C). To determine whether BMP2 mediates the ALKBH1-  
221 regulated VSMCs osteogenic reprogramming, mice primary VSMCs and aortic rings  
222 were infected with AAV sh-BMP2 together with AAV-ALKBH1. BMP2 knockdown  
223 effectively antagonized the ALKBH1-enhanced osteogenic reprogramming (Figure 6D)  
224 and mineralized nodule formation (Figure 6E), accompanied by decreased ALP activity  
225 (Figure 6F) and calcium content (Figure 6G). It has been previously reported that BMP2  
226 acts by inducing the expression of RUNX2 in VSMCs, thereby affecting osteogenic  
227 reprogramming (29). We observed that BMP2 depletion could decrease RUNX2  
228 upregulation, which indicated that BMP2 is the upstream regulator. Further real time  
229 PCR analysis revealed that *Bmp2* levels were transcriptionally regulated in vitro (Figure  
230 7A) and in vivo (Figure 7, B and C). In addition, ALKBH1 depletion had no effect on the  
231 stability of *Bmp2* mRNA (Figure 7D). Above all, these data indicate that ALKBH1-  
232 induced calcification is directly dependent on BMP2.

233

234 *6mA demethylation promotes octamer-binding transcription factor 4 (Oct4) binding to*  
235 *the BMP2 promoter and activates transcription.* Next, we sought to elucidate the  
236 mechanism by which ALKBH1 depletion downregulates BMP2. Bioinformatics screening  
237 indicated three 6mA peaks (marked as ChIP1, 2, and 3) that were induced by ALKBH1  
238 knockdown in the human *BMP2* gene (Figure 8A) (30). ChIP-qPCR confirmed that  
239 ALKBH1 silencing altered 6mA saturation in these three regions. However, only the first  
240 6mA peak was subjected to osteogenic stimulation due to Pi-induced reduction of 6mA  
241 enrichment (Figure 8B). According to the literature, DNA methylation may regulate  
242 transcription by interfering with transcription factor binding (31). The sequence of the  
243 first region from -2882 bp to -2300 bp of *BMP2* promoter was analyzed. A binding site of  
244 Oct4, also known as POU domain class 5 transcription factor 1 (POU5F1), was  
245 predicted based on JASPAR with a defined 99% profile score threshold. We found that  
246 the application of *OCT4* siRNA repressed BMP2 protein and mRNA expression in  
247 HASMCs (Figure 8, C and D). Furthermore, ChIP-qPCR with Oct4 pull-down further  
248 demonstrated that Pi-reduced 6mA modification facilitated Oct4 accumulation in the first  
249 region, whereas ALKBH1-silencing-increased 6mA modification abrogated this effect  
250 (Figure 8E). In other words, demethylation of the *BMP2* promoter results in enhanced  
251 Oct4 binding. Interestingly, the western blot results showed that neither ALKBH1  
252 knockdown nor high Pi condition altered total Oct4 protein level (Figure 8F).

253 To detect whether Oct4 binding regulates *BMP2* transcription, serial human *BMP2*  
254 promoter (-3319 bp)-driven luciferase reporter assay was conducted with or without  
255 Oct4 binding site (Figure 8G). As shown in Figure 8H, Oct4 induced robust luciferase  
256 expression in pGL3-Oct4-WT, whereas mutation suppressed luciferase activity,

257 suggesting that Oct4 binds directly to the *BMP2* promoter within the first 6mA peak  
258 region to regulate its transcription. Under Pi stimulation, *BMP2* activity was upregulated  
259 with the Oct4 (pGL3-Oct4-WT) but not with the mutation. In addition, this increase could  
260 be dramatically antagonized by ALKBH1 knockdown (Figure 8I). Taken together, 6mA  
261 demethylation by ALKBH1 promotes the binding of Oct4 to the *BMP2* promoter, thus  
262 increasing the transcriptional activity of *BMP2*.

263

264 *Oct4 mediates the regulation of ALKBH1 on BMP2*. To explore whether Oct4 is involved  
265 in the regulation of ALKBH1 on BMP2, we utilized aorta and primary cells from  
266 tamoxifen-induced *Oct4* knockout mice. Aortic rings from *Oct4*<sup>WT/WT</sup>-Myh11-Cre/ERT2  
267 (WT) and *Oct4*<sup>F/F</sup>-Myh11-Cre/ERT2 (*Oct4*<sup>-/-</sup>) mice were cultured in an osteogenic  
268 medium for 14 days. Von Kossa staining (Figure 9, A and B) and calcium content  
269 quantification (Figure 9C) results showed decreased calcification in *Oct4*<sup>-/-</sup> mice. This  
270 observation was reinforced by transfection AAV-Vector or AAV-ALKBH1 into calcified  
271 primary VSMCs from WT or *Oct4*<sup>-/-</sup> mice. Depletion of Oct4 significantly alleviated the  
272 pro-calcifying effect of ALKBH1 overexpression by downregulating BMP2 protein and  
273 mRNA expressions (Figure 9, D-G). Based on these findings, we concluded that Oct4  
274 mediates the regulation of ALKBH1 on BMP2.

275

276

277 **Discussion**

278 The heterogeneity of VSMCs and their tight communication with the bloodstream render  
279 it challenging to uncover the mechanism underlying VC (1). In the current study, we  
280 found that the DNA 6mA levels in leukocytes and VSMCs were dynamically decreased  
281 along with calcification progression in CKD. This suggests a potential role of DNA 6mA  
282 modification in calcification formation. Upregulation of ALKBH1, but not N6AMT1,  
283 mediates this observed 6mA reduction. Moreover, *in vivo* gain- and loss-of-function  
284 experiments showed that ALKBH1 deficiency in VSMCs bestows a strong anti-  
285 calcification effect, while exogenous overexpression of ALKBH1 augmented calcification  
286 formation. Mechanistically, ALKBH1-demethylated DNA 6mA could facilitate Oct4  
287 binding to *BMP2* promoter and subsequently increase *BMP2* transcription, which  
288 resulted in osteogenic reprogramming of VSMCs and VC progression. Taken together,  
289 these results demonstrate that the ALKBH1 acts as a catastrophic trigger for VC.

290 Mounting evidence supports a critical role of DNA methylation and demethylation in  
291 VSMCs phenotypic transition due to environmental signal modulation (32). Previous  
292 research has focused mainly on canonical 5mC due to its abundance and significance  
293 in eukaryotes. A set of VSMCs contractile and osteogenic genes, including klotho (12),  
294 *TAGLN* (15), and peroxisome proliferator-activated receptor gamma (33) are regulated  
295 by DNA 5mC methylation that could be consequently associated with VSMCs  
296 phenotypic transition and pathogenesis of VC. In addition to the genome-wide DNA  
297 5mC, recently ALKBH1-mediated 6mA DNA demethylation was identified in human  
298 cardiovascular diseases (19). However, it remains unknown whether VSMCs can adopt  
299 novel epigenetic mechanisms that are rarely utilized in normal human tissues during VC.

300 Here, we took advantage of the ELISA to quantify the level of DNA 6mA modification in  
301 vivo and in vitro. Previous epigenome-wide association studies (EWASs) based on  
302 whole blood DNA methylation have identified numerous CpG sites that are associated  
303 with aging (34) and all-cause mortality (35). In this study, we demonstrated that 6mA  
304 levels were significantly decreased in leukocytes and radial arteries from CKD patients  
305 with VC, as well as the CKD mice.

306 Human and murine leukocyte DNA 6mA levels measured in our study were  
307 approximately 0.04% of the total adenines, which is comparable with previous research  
308 (17). Our findings suggested that epigenetic DNA 6mA modifications occurred  
309 systemically in response to the CKD-induced hyperphosphatemia, both in circulating  
310 leukocytes and in situ VSMCs. Moreover, 6mA levels in the CKD mouse model  
311 exhibited a similar decreasing pattern with humans. Therefore, leukocyte DNA 6mA  
312 modification levels, at least in part, may reflect the corresponding systematic change of  
313 6mA modification in VSMCs. Calcium deposition in the arterial wall is considered a  
314 typical feature for VC. As we observed, the calcification Agatston score and Volume  
315 score of aortic arch exhibited a negative and positive correlation with 6mA and ALKBH1  
316 levels in leukocytes from CKD patients, respectively. As the severity of calcification  
317 increases, 6mA levels narrow between different stages of VC progression. These  
318 interpretations are limited, as the findings in CKD patients with VC are observational  
319 due to insufficient access to direct tissue artery biopsies. Despite these limitations, our  
320 preclinical studies provide at least preliminary indications that DNA 6mA levels may  
321 function as a novel epigenetic biomarker for early diagnosis of VC initiation since  
322 regular MDCT does not have the sensitivity to identify minor aortic calcification lesion.

323 Leukocyte isolation and analysis could be a simple yet highly effective clinical approach  
324 since MDCT contrast agents may have adverse effects on uremic patients.

325 Gain- and loss-of-function experiments corroborated the evidence for causal ALKBH1  
326 involvement in VC. ALKBH1 deficiency in VSMCs significantly alleviated the  
327 accumulation of calcium deposition in the arterial wall, while ALKBH1 overexpression  
328 exacerbated this pathological process. Specific mediators such as SOX9, DLX5,  
329 RUNX2, and BMP2, are involved in VSMCs osteogenic reprogramming and calcification  
330 development (36). Here, we found that BMP2 expression was significantly blunted by  
331 ALKBH1 deficiency in calcified VSMCs. Moreover, the notable pro-calcifying outcome  
332 arising from ALKBH1 overexpression was abolished upon BMP2 depletion. That said,  
333 ALKBH1-mediated VC is dependent on BMP2. However, the mechanism by which  
334 ALKBH1 downregulates VSMCs contractile markers under high phosphate stimulation  
335 is not fully understood. Interestingly, previous work found that BMP2 could repress  
336 *TAGLN* promoter activity in VSMCs via a common cis-acting transforming-growth-factor-  
337 control element, which is present in promoter regions of multiple contractile VSMCs  
338 gene (37).

339 Thus, a critical question to consider is how ALKBH1 regulates BMP2 expression. In  
340 mouse embryonic stem cells (mESCs), 6mA was enriched at young long interspersed  
341 nuclear element 1 transposon, and its deposition correlates with epigenetic silencing  
342 (38). Recent studies have also shown that 6mA affects gene expression by regulating  
343 the binding of specific transcription factor to the target gene promoter region (18, 39).  
344 Our results revealed that Pi induced ALKBH1-demethylated 6mA on an Oct4 binding  
345 region within the *BMP2* promoter, which facilitated Oct4 binding and promoted *BMP2*

346 transcriptional activation. Although the Oct4 binding motif has multiple adenosines that  
347 are required for Oct4 binding, we acknowledge that a limitation of the current study is  
348 that we could not precisely identify which adenosine undergoes N<sup>6</sup> methylation. Recent  
349 sequencing technology could not distinguish genomic 6mA and adenosine. In addition,  
350 application of VSMC-specific *Alkbh1* gene knockout mice will be better to bolster our  
351 findings.

352 In summary, our clinical investigation established an association of dynamically  
353 decreased DNA 6mA modification with the progression of VC. Our mechanistic results  
354 demonstrated the pro-calcification impact of ALKBH1-demethylated DNA 6mA  
355 modification in CKD. From a clinical standpoint, these observations warrant further  
356 study of DNA 6mA level as an early-diagnosis approach and ALKBH1 inhibition as a  
357 potential therapeutic strategy for the prevention of VC.

358

359 **Methods**

360 *Study population and patient artery samples.* This case-control study was conducted  
361 from March 2018 to January 2020 in the Donghua Hospital of Sun Yat-sen University,  
362 China. A total of 198 patients diagnosed with CKD were recruited in our study. We  
363 excluded 10 patients who met the exclusion criteria and 15 patients who missed the  
364 data of MDCT or plasma biomedical tests. Clinical and biochemical parameters were  
365 collected from the electronic medical record in the hospital.

366 The diagnosis of CKD was based on eGFR decline present for  $\geq$  6 months. CKD stage  
367 1 to 2 was defined as albumin/creatinine ratio (ACR) (mg/g)  $\geq$  17 in men and  $\geq$  25 in  
368 women, and an eGFR  $\geq$  60 ml/min per 1.73 m<sup>2</sup> following the Kidney Disease Outcomes  
369 Quality Initiative (K/DOQI) guidelines (40). CKD stage 3 to 5 was defined as an  
370 estimated GFR  $<$  60 ml/min per 1.73 m<sup>2</sup> among study participants before receiving  
371 dialysis. Patients were excluded if: (1) with age  $<$ 18 and  $\geq$  90 years; (2) pregnant; (3)  
372 administration of any medication as phosphate binders, vitamin D analogs or the  
373 corticosteroids within 3 months before recruitment; (4) acute renal failure; (5)  
374 uncontrolled hyperlipidemia and (6) history of hepatic diseases or neoplastic disease.

375 A 4-6 mm segment of the radial artery was removed from CKD patients who underwent  
376 an arterial venous fistula operation with diagnosed aortic arch calcification (CKD, n = 10)  
377 or from patients who underwent amputation surgery due to upper limb trauma without  
378 diagnosed CKD or diabetes mellitus (Control, n = 8). Fat and adventitia were removed  
379 from samples before storing them at liquid nitrogen.

381 **Assessment of calcification score.** Among the cohort, all patients underwent a chest  
382 MDCT scanning with standard electrocardiographically (ECG)-gated protocol to  
383 evaluate aortic arch calcification. All the Agatston and Volume scores of images were  
384 blindingly quantified by two independent investigators with Siemens Syngo CT  
385 Workplace software according to standard criteria (41). The aortic arch refers to the part  
386 between the ascending and descending aorta. To measure the calcification scores, the  
387 CT images were reconstructed with slices of 1 mm thickness. The presence of  
388 calcification was defined as an Agatston score or Volume score > 0 in the present study.  
389 Studies focused on coronary artery describing Agatston scores > 400 as severe  
390 calcification (42-44). Considering the higher calcification scores in aortic arch (Agatston  
391 score [median, 411]; Volume score [median, 461]) than coronary artery (Agatston score  
392 [median, 163]; Volume score [median, 283]), patients were divided into non-VC (Agatston  
393 score or Volume score = 0), mild (500 ≥ Agatston score or Volume score > 0), or severe  
394 (Agatston score or Volume score > 500) subgroups as previously described (45).  
395 Calcification scores was adjusted with a calcium standard calibration phantom that was  
396 scanned along with the participant (46). In addition, calcification scores and the relevant  
397 statistical analyses were adjusted for age, sex and ethnicity (47).

398

399 **Laboratory analyses.** An overnight fasting median cubital venous blood was collected  
400 for analyses of biochemical parameters from CKD patients before dialysis. Leukocyte  
401 cells were isolated for subsequent DNA and RNA analyses. Plasma levels of potassium,  
402 calcium, phosphate, blood urea nitrogen (BUN), Creatinine (CREA), uric acid (URCA),  
403 albumin (ALB), alanine transaminase (ALT), aspartate aminotransferase (AST), alkaline

404 phosphatase (ALP), cholesterol (CHOL), triglyceride (TG), high-density lipoprotein  
405 cholesterol (HDL-C), low-density lipoprotein cholesterol (LDL-C) were analyzed using  
406 the standard certified TBA-120 auto-analyzer (Toshiba Medical Systems, Japan) in the  
407 Central Clinical Laboratory at Donghua Hospital of Sun Yat-sen University. The suPAR  
408 in plasma were measured by the detection kit (ViroGates) according to the  
409 manufacturer's instructions. The estimated glomerular filtration rate was assessed using  
410 the modified Modification of Diet in Renal Disease (MDRD) equation for the Chinese  
411 population (48).

412

413 *Quantification of 6mA DNA methylation.* The DNeasy Blood & Tissue Kit from Qiagen  
414 (USA, CA) was used to extract genomic DNA from peripheral blood specimens of  
415 humans and mice and cultured cell lines. The integration of genomic DNA was  
416 confirmed on an agarose gel, and the concentration was measured by a NanoDrop  
417 spectrophotometer. 6mA DNA methylation level was quantified by Methyl Flash 6mA  
418 DNA Methylation Enzyme-Linked Immunosorbent Assay (ELISA) Kit (Colorimetric) from  
419 Epigentek (USA, NY) following the manufacturer's protocol. In brief, the methylated  
420 fraction of a total of 100 ng of genomic DNA was recognized by a 6mA antibody and  
421 quantified by an ELISA-like reaction. The percentage of 6mA (6mA %) was calculated  
422 by optical density (OD) value according to the recommended formula. Methylated and  
423 unmethylated DNA were incubated each test as a positive and negative control,  
424 respectively. Each sample ran in duplicate.

425

426 *Chemicals and antibodies.* Adenine (A8626),  $\beta$ -GP (G9422) and L-ascorbic acid (A4544)  
427 were purchased from Sigma-Aldrich (MO, USA). For western blot (WB),  
428 immunofluorescence (IF), and immunohistochemistry (IHC), antibodies against RUNX2  
429 (12556S; 1:1000 for WB), SOX9 (82630S; 1:1000 for WB) and Calponin1 (17819S;  
430 1:1000 for WB) were obtained from Cell Signaling Technology (MA, USA). Antibodies  
431 against  $\alpha$ -SMA (ab7817; 1:2000 for WB; 1:100 for IF), BMP2 (ab14933; 1:1000 for WB;  
432 1:100 for IF), SM22 $\alpha$  (ab14106; 1:2000 for WB), OPN (ab8448; 1:1000 for WB) and  
433 Oct4 (ab19857; 1:500 for WB) were purchased from Abcam (Cambridge, UK).  
434 Antibodies against Collagen I (NB600-408; 1:1000 for WB) was purchased from Novus  
435 (CO, USA). Antibodies against ALKBH1 (OACA06689; 1:1000 for WB; 1:100 for IF and  
436 IHC) and N6AMT1 (OAAN02175; 1:1000 for WB; 1:100 for IF and IHC) were obtained  
437 from Aviva Systems Biology (CA, USA). Antibodies against 6mA (ABE572; 1:100 for IF  
438 and IHC) for ChIP were obtained from EMD Millipore (MA, USA), and Oct4 (2750S) for  
439 ChIP were purchased from Cell Signaling Technology (MA, USA). The OCN (sc-390877;  
440 1:500 for WB), DXL5 (sc-398150; 1:500 for WB), GAPDH (sc-32233; 1:1000 for WB)  
441 and  $\beta$ -Actin (sc-47778; 1:1000 for WB) antibody was purchased from Santa Cruz  
442 Biotechnology (TX, USA).

443  
444 *Animal experiments.* Eight-week-old male C57BL/6J mice were purchased from  
445 Laboratory Animal Center of Sun Yat-sen University.  $Oct4^{F/F}$  (Pou5f1<sup>tm1Scho</sup>) and Myh11-  
446 Cre/ERT2 mice were purchased from the Jackson Laboratory (USA, ME) to generate  
447  $Oct4^{F/F}$ -Myh11-Cre/ERT2 mice. Cre mediated recombination was achieved via 10 daily  
448 intraperitoneal injections of tamoxifen (Sigma, UAS) at six-week-age. Male  $Oct4^{WT/WT}$ -

449 Myh11-Cre/ERT2 were referred as WT, and tamoxifen-injected male *Oct4*<sup>F/F</sup>-Myh11-  
450 Cre/ERT2 mice were referred as *Oct4*<sup>-/-</sup> for simplicity. All mice were housed in a  
451 temperature-controlled environment under a 12-hour light cycle, and they had free  
452 access to water and the assigned diet. For adenine-diet-induced CKD model, mice were  
453 randomly provided with a chow diet as the control group, or a special diet containing 0.2%  
454 adenine, 1.2% phosphorus as CKD group (49-52) . For 5/6-nephrectomy-induced CKD  
455 model, we followed a modified protocol based on the well-established two-step  
456 procedure we used in rats (53-55). Briefly, anesthesia was induced in eight-week-old  
457 male mice with isoflurane (induction 5%, maintenance 2%). Firstly, the upper and lower  
458 poles of left kidney were ligated and excised under microscope. Thus, two-third of the  
459 left kidney were removed. One week later, mice were subjected to removal of right  
460 kidney to achieve 5/6 nephrectomy. 4 weeks after initiation of the special diet or first-  
461 step surgery, mice were injected with the indicated virus ( $5 \times 10^9$  plaque-forming units  
462 per kilogram per mouse) via tail vein, respectively, as previously described (56, 57).  
463 Four weeks later, mice were fasted overnight and weighted before euthanasia, and  
464 blood was collected and separated into plasma and leukocytes. Blood levels of fast  
465 blood glucose, phosphorus, creatinine, and urea BUN were measured by the  
466 autoanalyzer (Hitachi, Japan). Plasma cholesterol and triglyceride were measured using  
467 specific reagents (Infinity<sup>TM</sup>, Thermo). Plasma levels of calcium were measured using  
468 the detection kit (Abcam, ab102505). Plasma levels of ALP were measured using the  
469 detection kit (QuantiChrom<sup>TM</sup>, DALP-250). The suPAR in plasma was measured by the  
470 detection kit (R&D, DY531) according to the manufacturer's instructions. Whole aortas  
471 were harvested and carefully dissected for further analyses.

472

473 *Blood pressure.* Measurements of systolic blood pressure (SBP) and diastolic blood  
474 pressure (DBP) in mice were performed by non-invasive tail cuff plethysmography  
475 (CODA, Kent Scientific Corporation), before (W0), 2 (W2) and 4 (W4) weeks after virus  
476 injection. These measurements were conducted in conscious and trained mice in the  
477 morning with 5 acclimation cycles followed by 15 measurement cycles. The mean value  
478 of measurements was used for comparison.

479

480 *Immunohistochemistry.* Vascular sections (5  $\mu\text{m}$ ) were deparaffinized and rehydrated.  
481 Endogenous peroxidase activity was blocked using 0.3%  $\text{H}_2\text{O}_2$  at room temperature for  
482 20 minutes. Heat-mediated antigen retrieval was performed using 10% citrate buffer.  
483 Sections were stained with primary antibodies overnight at 4°C followed with EnVision+  
484 Dual Link System-HRP (Dako, CH) and visualized with diaminobenzidine. OLYMPUS  
485 BX51 microscope (Japan) was used for image collecting, and the scores were  
486 calculated by the percentages of positive cells and staining intensities as previously  
487 described (58).

488

489 *Immunofluorescence.* Slides (8  $\mu\text{m}$ ) were washed with diluted water and fixed in iced  
490 acetone for 10 minutes and then blocked with goat serum. Slides were incubated with  
491 antibodies at 4°C overnight and then incubated with Alexa Fluor® (Jackson  
492 ImmunoResearch, USA) secondary antibodies for one hour at 37°C. Nuclei were  
493 stained with DAPI. Images were acquired by OLYMPUS fluorescence microscope and  
494 quantified by Image-Pro Plus 6.0 (Media Cybernetics, USA).

495

496 *Histological examination.* Kidney was fixed in 10% formalin and embedded in paraffin.  
497 Sagittal sections were stained with hematoxylin and eosin (H&E) for morphology using  
498 solution from Sigma Aldrich (USA, MO), Sirus red for fibrosis using stain kit  
499 (Polysciences, 24901), and von Kossa staining for mineral deposition (American  
500 MasterTech Scientific, KTVKO) according to the manufacturer's instructions.

501

502 *Ex vivo cell and vascular tissue culture.* Primary murine VSMCs were isolated from  
503 aortas of eight-week-old male C57BL/6J mice, twelve-week-old male  $Oct4^{WT/WT}$ -Myh11-  
504 Cre/ERT2 mice or tamoxifen-pretreated twelve-week-old male  $Oct4^{F/F}$ -Myh11-Cre/ERT2  
505 mice, respectively, and cultured in a growth medium as described by Hou et al (59).  
506 Human aortic smooth muscle cells (HASMCs) were purchased from the American Type  
507 Culture Collection (MD, USA) and cultured in M231 medium (Life Technology, USA)  
508 containing 10% fetal bovine serum (FBS) (GIBCO, USA). All experiments were  
509 performed with VSMCs at passages 3 to 6. Mice aortic arteries were dissected under  
510 sterile conditions from eight-week-old male C57BL/6J mice, twelve-week-old male  
511  $Oct4^{WT/WT}$ -Myh11-Cre/ERT2 mice or tamoxifen-pretreated twelve-week-old male  
512  $Oct4^{F/F}$ -Myh11-Cre/ERT2 mice, respectively. After removing the adventitia, the vessels  
513 were cut into 2-3 mm rings and placed in Dulbecco's Modified Eagle's Medium (DMEM)  
514 (GIBCO, USA) containing 10% FBS.

515 Cells were transfected with control siRNA, *ALKBH1* or *OCT4* siRNA (Santa Cruz  
516 Biotechnology, USA) accordingly with Lipofectamine RNAiMAX Reagent (Invitrogen,  
517 USA) as we described (60). Plasmids were transfected into HASMCs by electroporation

518 using the P1 Primary Cell 4D-Nucleofector X Kit L from Lonza (MD, USA) following  
519 manufacturer's instruction. For indicated viruses, cells were seeded overnight prior to  
520 viral infections. The efficiency of transfection was determined by real-time polymerase  
521 chain reaction (PCR) or western blot.

522

523 *In vivo calcification quantification.* Calcification was identified by von Kossa stain and  
524 analyzed by ImageJ (NIH Bethesda, USA). Aortic sections were treated with 5% silver  
525 nitrate and exposed to ultraviolet light for 30 minutes, rinsed, and incubated with 5%  
526 sodium thiosulfate. Calcified spots were stained brown. The aortic arch was decalcified  
527 with 0.6 mmol/L hydrochloric acid at 37°C for 48 hours. Released calcium was  
528 quantified using the Calcium Assay Kit (Abcam, ab102505) in compliance with the  
529 manufacturer's protocol. The content of calcium was normalized by the dry weight of  
530 vascular tissues. The presence of calcification was defined by positive von Kossa  
531 staining in the medial aortic layer as calcification lesion size (% of SMC layer) > 0 in this  
532 study. Mice were divided into non-VC (calcification lesion size = 0), mild (10% ≥  
533 calcification lesion size > 0) or severe (calcification lesion size > 10%) subgroup.

534

535 *In vitro calcification quantification.* Cells or aortic rings were cultured in an osteogenic  
536 medium containing 0.25mmol/L L-ascorbic acid and 10mmol/L  $\beta$ -glycerophosphate for  
537 14 days to induce in vitro calcification. Calcification was determined by Alizarin red stain  
538 (Thermo Fisher Scientific, AA42746AP) as described previously (60). Positively stained  
539 cells showed a red color. The calcium deposition in the plate was decalcified and  
540 subjected to colorimetric analysis using a Calcium Assay Kit (Abcam, ab102505) and

541 calibrated to the protein content (60). In parallel duplicate, ALP activity was measured  
542 using an ALP assay kit (QuantiChrom, DALP-250) and normalized to the levels of total  
543 protein according to the manufacturer's instructions.

544

545 *Quantitative real time PCR.* Total RNA from peripheral leukocytes, cultured cells, or  
546 murine aortas were extracted with TRIzol (Invitrogen, USA) and reverse-transcribed into  
547 cDNA with iScript cDNA Synthesis Kits (Bio-Rad, USA). PCR amplification was  
548 performed using Bio-Rad SYBR Green on a CFX96 Touch Real-Time PCR Detection  
549 System (Bio-Rad, USA). The relative mRNA levels were calibrated by the housekeeping  
550 gene GAPDH. The primers were listed in Supplemental Table 4.

551

552 *Western blotting analysis.*

553 Cell lysates or aortic homogenates were performed western blot analysis as previously  
554 described (60). The intensity of the individual band was quantified by densitometry  
555 using ImageJ (NIH Bethesda, USA).

556

557 *Chromatin immunoprecipitation (ChIP)-qPCR.* The bioinformatics screening of  
558 functional 6mA binding sites was obtained from the NCBI GEO DataSets (GSE118093).  
559 ChIP analyses were performed using the Simple Chip Enzymatic Chromatin  
560 immunoprecipitation kit (Cell Signaling Technology, 9002S) following the manufacturer's  
561 protocols. Briefly, treated cells were crosslinked with formaldehyde and then quenched  
562 by glycine, finally digested with micrococcal nuclease. The lysates were  
563 immunoprecipitated with 5 µg rabbit anti-IgG, anti-6mA or anti-Oct4 antibody overnight

564 at 4°C, followed by incubation with 50µL ChIP-Grade Protein G Agarose beads (Cell  
565 Signaling Technology, 9007S) for 2h at 4°C with gentle rotation. The crosslinked DNA  
566 fragments were eluted, reversed, and purified. ChIP DNA was amplified by real time  
567 PCR with designed primers (Supplemental Table 4). 2% amount of each reaction was  
568 used as an input reference. The results were analyzed by the following formula: percent  
569 Input = 2% x 2<sup>(Ct 2%Input Sample – Ct IP Sample)</sup>.

570

571 *Recombinant adeno-associated virus construction.* To generate AAV encoding mouse  
572 *Alkbh1* (NM\_001102565.1), the genomic AAV vector, AAV helper plasmid, and AAV  
573 serotype 2 plasmid (Origene, USA) were co-transfected into HEK293 cells (American  
574 Type Culture Collection, USA), and the harvested viral particles were purified as  
575 outlined previously (59, 61). Double digestion was done with Sgfl and MluI restriction  
576 enzymes (Sigma-Aldrich, USA) to remove the *Alkbh1* open reading frame clone from  
577 pCMV6-Myc-DDK-*Alkbh1* plasmid (Origene, MR222060) to construct genomic AAV  
578 vector. In order to construct optimal AAV expressing shRNA against *Alkbh1* and *Bmp2*,  
579 three lines of the corresponding AAV were modified and packaged and then transfected  
580 into murine VSMCs to determine the efficiency of knockdown (Supplemental Figure 11).  
581 The optimal sequences were listed as follows: *Alkbh1* shRNA with the sense  
582 oligonucleotides 5'-CCGGGAAATACTCAGCAGATCATTACTCGAGTAATGATCTGCT  
583 GAGTATTCTTTTG-3'; and *Bmp2* shRNA with the sense oligonucleotides 5'-  
584 CCGGCCTCCGGGCTATCATGCCTTCTCGAGAAAGGCATGATAGCCGGAGGTTT  
585 T-3'. To ensure the restricted genomic manipulation in the smooth muscle cell, all the  
586 AAV vectors were ligated with *Tagln* promoter.

587

588 *Plasmid construction and luciferase reporter assay.* The serial DNA fragments from the  
589 human *BMP2* promoter (-3319 bp) were amplified by PCR. The PCR product was  
590 digested with Sac I and Hind III (Sigma-Aldrich, USA) and cloned into pGL3-Vector to  
591 generate the *BMP2* luciferase reporter constructs. Mutant constructs of the deleted  
592 binding site for Oct4 in the *BMP2* promoter were generated by designed primers. The  
593 constructs were verified by sequencing. Followed by the indicated treatment, the  
594 reporter plasmid was co-transfected with internal control Renilla luciferase plasmid  
595 (Promega, USA) into HASMCs by electroporation. Transcriptional activity was detected  
596 by the Dual-Luciferase Reporter Assay Kit obtained from Promega (WI, USA) according  
597 to the manufacturer's instructions. The related primers were listed in Supplemental  
598 Table 4.

599

600 *Lentivirus transfection.* HASMCs were infected with recombinant lentivirus expressing  
601 control shRNA (Santa Cruz Biotechnology, sc-108080), *ALKBH1* shRNA (Santa Cruz  
602 Biotechnology, sc-60153-V) according to the manufacturer's instruction. Colonies were  
603 selected by treatment with 5 $\mu$ g/mL puromycin (Sigma-Aldrich, USA) for 7 days.

604

605 *Statistical analyses.* All analyses were performed with SPSS 23.0 software (SPSS Inc.).  
606 Values are expressed as means  $\pm$  standard deviation. For comparisons between two  
607 groups, significance was determined using Student's t-test or nonparametric Mann–  
608 Whitney test. For comparisons among multiple groups, ANOVA was performed, followed  
609 by the post hoc Bonferroni test or Dunnett's test. The statistical significance of

610 correlations was assessed by Pearson's correlation coefficient analysis. Two-tailed  $p <$   
611 0.05 (indicated by \*, # or †) was considered statistically significant.

612

613 *Study approval.* The protocol for clinical study conformed to the ethical guidelines of the  
614 1975 Declaration of Helsinki and was approved by the Ethics Committee of the  
615 Donghua Hospital of Sun Yat-sen University. All participants signed informed consent  
616 before entering this study. Written informed consent was provided for pictures appearing  
617 in the manuscript. The experimental animal protocols were reviewed and approved by  
618 the Ethics Committee of Zhongshan School of Medicine, Sun Yat-sen University.

619

620 **Author contributions**

621 LO and HH designed the research; LO, MZ, and WL performed the experiments; LO,  
622 XS, LT, YZ, PZ, CX, and JC analyzed and interpreted the data; and LO and H.H. wrote  
623 the manuscript with comments from all authors; all authors approved the final version of  
624 the manuscript.

625

626 **Acknowledgements**

627 This work was supported by the National Natural Science Foundation of China  
628 (8201101103, 81870506 and 81670676), Project of Traditional Chinese Medicine in  
629 Guangdong Province (20201062), Basic Research Project of Shenzhen Science and  
630 Technology Innovation Committee (JCYJ20180306174648342 and  
631 JCYJ20190808102005602), Shenzhen Futian District Public Health Research Project  
632 (FTWS2019003), and Shenzhen Key Medical Discipline Construction Fund (SZXK002)  
633 to HH. In addition, this work was supported by the National Natural Science Foundation  
634 of China 82073408 to JC and Dongguan Social Science and Technology Development  
635 Project (2018507150461629) to XS.

636

637 **References**

638

639 1. Blaha MJ, et al. Associations between C-reactive protein, coronary artery calcium,  
640 and cardiovascular events: implications for the JUPITER population from MESA,  
641 a population-based cohort study. *Lancet*. 2011;378(9792):684-692.

642 2. Timmis A, et al. European Society of Cardiology: Cardiovascular Disease  
643 Statistics 2017. *Eur Heart J*. 2018;39(7):508-579.

644 3. Moe SM, and Chen NX. Mechanisms of vascular calcification in chronic kidney  
645 disease. *J Am Soc Nephrol*. 2008;19(2):213-216.

646 4. Guerin AP, et al. Impact of aortic stiffness attenuation on survival of patients in  
647 end-stage renal failure. *Circulation*. 2001;103(7):987-992.

648 5. Pursnani A, et al. Guideline-Based Statin Eligibility, Coronary Artery Calcification,  
649 and Cardiovascular Events. *JAMA*. 2015;314(2):134-141.

650 6. Lanzer P, et al. Medial vascular calcification revisited: review and perspectives.  
651 *Eur Heart J*. 2014;35(23):1515-1525.

652 7. Iribarren C, et al. Calcification of the aortic arch: risk factors and association with  
653 coronary heart disease, stroke, and peripheral vascular disease. *JAMA*.  
654 2000;283(21):2810-2815.

655 8. Opdebeeck B, et al. Indoxyl Sulfate and p-Cresyl Sulfate Promote Vascular  
656 Calcification and Associate with Glucose Intolerance. *J Am Soc Nephrol*.  
657 2019;30(5):751-766.

658 9. Shroff R, et al. Mechanistic insights into vascular calcification in CKD. *J Am Soc  
659 Nephrol*. 2013;24(2):179-189.

660 10. Salazar VS, et al. BMP signalling in skeletal development, disease and repair.  
661 *Nat Rev Endocrinol.* 2016;12(4):203-221.

662 11. Li X, et al. BMP-2 promotes phosphate uptake, phenotypic modulation, and  
663 calcification of human vascular smooth muscle cells. *Atherosclerosis.*  
664 2008;199(2):271-277.

665 12. Chen J, et al. Indoxyl Sulfate Enhance the Hypermethylation of Klotho and  
666 Promote the Process of Vascular Calcification in Chronic Kidney Disease. *Int J*  
667 *Biol Sci.* 2016;12(10):1236-1246.

668 13. Pons D, et al. Epigenetic histone acetylation modifiers in vascular remodelling:  
669 new targets for therapy in cardiovascular disease. *Eur Heart J.* 2009;30(3):266-  
670 277.

671 14. Goetsch C, et al. MicroRNA in cardiovascular calcification: focus on targets and  
672 extracellular vesicle delivery mechanisms. *Circ Res.* 2013;112(7):1073-1084.

673 15. Montes de Oca A, et al. High-phosphate-induced calcification is related to  
674 SM22alpha promoter methylation in vascular smooth muscle cells. *J Bone Miner*  
675 *Res.* 2010;25(9):1996-2005.

676 16. Zhu S, et al. Mapping and characterizing N6-methyladenine in eukaryotic  
677 genomes using single-molecule real-time sequencing. *Genome Res.*  
678 2018;28(7):1067-1078.

679 17. Xiao CL, et al. N(6)-Methyladenine DNA Modification in the Human Genome. *Mol*  
680 *Cell.* 2018;71(2):306-318 e307.

681 18. Wu L, et al. Association of N(6)-methyladenine DNA with plaque progression in  
682 atherosclerosis via myocardial infarction-associated transcripts. *Cell Death Dis.*

683 2019;10(12):909.

684 19. Guo Y, et al. DNA N(6)-methyladenine modification in hypertension. *Aging*  
685 (Albany NY). 2020;12(7):6276-6291.

686 20. Zhou C, et al. DNA N(6)-methyladenine demethylase ALKBH1 enhances  
687 osteogenic differentiation of human MSCs. *Bone Res.* 2016;4:16033.

688 21. Xie SA, et al. Matrix stiffness determines the phenotype of vascular smooth  
689 muscle cell in vitro and in vivo: Role of DNA methyltransferase 1. *Biomaterials*.  
690 2018;155:203-216.

691 22. Hadji F, et al. Altered DNA Methylation of Long Noncoding RNA H19 in Calcific  
692 Aortic Valve Disease Promotes Mineralization by Silencing NOTCH1. *Circulation*.  
693 2016;134(23):1848-1862.

694 23. Azam TU, et al. Soluble Urokinase Receptor (SuPAR) in COVID-19-Related AKI.  
695 *J Am Soc Nephrol.* 2020;31(11):2725-2735.

696 24. Hahm E, et al. Bone marrow-derived immature myeloid cells are a main source  
697 of circulating suPAR contributing to proteinuric kidney disease. *Nat Med.*  
698 2017;23(1):100-106.

699 25. Hayek SS, et al. A tripartite complex of suPAR, APOL1 risk variants and  
700 alphavbeta3 integrin on podocytes mediates chronic kidney disease. *Nat Med.*  
701 2017;23(8):945-953.

702 26. Hayek SS, et al. Soluble Urokinase Receptor and Acute Kidney Injury. *N Engl J*  
703 *Med.* 2020;382(5):416-426.

704 27. Hayek SS, et al. Soluble Urokinase Receptor and Chronic Kidney Disease. *N*  
705 *Engl J Med.* 2015;373(20):1916-1925.

706 28. Ougland R, et al. ALKBH1 is a histone H2A dioxygenase involved in neural  
707 differentiation. *Stem Cells*. 2012;30(12):2672-2682.

708 29. Rong S, et al. Vascular calcification in chronic kidney disease is induced by bone  
709 morphogenetic protein-2 via a mechanism involving the Wnt/beta-catenin  
710 pathway. *Cell Physiol Biochem*. 2014;34(6):2049-2060.

711 30. Xie Q, et al. N(6)-methyladenine DNA Modification in Glioblastoma. *Cell*.  
712 2018;175(5):1228-1243 e1220.

713 31. Poetsch AR, and Plass C. Transcriptional regulation by DNA methylation. *Cancer*  
714 *Treat Rev*. 2011;37 Suppl 1:S8-12.

715 32. Alexander MR, and Owens GK. Epigenetic control of smooth muscle cell  
716 differentiation and phenotypic switching in vascular development and disease.  
717 *Annu Rev Physiol*. 2012;74:13-40.

718 33. Liu L, et al. High phosphate-induced downregulation of PPARgamma contributes  
719 to CKD-associated vascular calcification. *J Mol Cell Cardiol*. 2018;114:264-275.

720 34. Hannum G, et al. Genome-wide methylation profiles reveal quantitative views of  
721 human aging rates. *Mol Cell*. 2013;49(2):359-367.

722 35. Zhang Y, et al. DNA methylation signatures in peripheral blood strongly predict  
723 all-cause mortality. *Nat Commun*. 2017;8:14617.

724 36. Thompson B, and Towler DA. Arterial calcification and bone physiology: role of  
725 the bone-vascular axis. *Nat Rev Endocrinol*. 2012;8(9):529-543.

726 37. King KE, et al. Kruppel-like factor 4 (KLF4/GKLF) is a target of bone  
727 morphogenetic proteins and transforming growth factor beta 1 in the regulation of  
728 vascular smooth muscle cell phenotype. *J Biol Chem*. 2003;278(13):11661-11669.

729 38. Wu TP, et al. DNA methylation on N(6)-adenine in mammalian embryonic stem  
730 cells. *Nature*. 2016;532(7599):329-333.

731 39. Li Z, et al. Epigenetic Methylations on N6-Adenine and N6-Adenosine with the  
732 same Input but Different Output. *Int J Mol Sci*. 2019;20(12).

733 40. National Kidney F. K/DOQI clinical practice guidelines for chronic kidney disease:  
734 evaluation, classification, and stratification. *Am J Kidney Dis*. 2002;39(2 Suppl  
735 1):S1-266.

736 41. Agatston AS, et al. Quantification of coronary artery calcium using ultrafast  
737 computed tomography. *J Am Coll Cardiol*. 1990;15(4):827-832.

738 42. Budoff MJ, et al. Testosterone Treatment and Coronary Artery Plaque Volume in  
739 Older Men With Low Testosterone. *JAMA*. 2017;317(7):708-716.

740 43. Budoff MJ, et al. Prognostic Value of Coronary Artery Calcium in the PROMISE  
741 Study (Prospective Multicenter Imaging Study for Evaluation of Chest Pain).  
742 *Circulation*. 2017;136(21):1993-2005.

743 44. Raggi P, et al. Identification of patients at increased risk of first unheralded acute  
744 myocardial infarction by electron-beam computed tomography. *Circulation*.  
745 2000;101(8):850-855.

746 45. Odink AE, et al. Association between calcification in the coronary arteries, aortic  
747 arch and carotid arteries: the Rotterdam study. *Atherosclerosis*. 2007;193(2):408-  
748 413.

749 46. Nelson JC, et al. Measuring coronary calcium on CT images adjusted for  
750 attenuation differences. *Radiology*. 2005;235(2):403-414.

751 47. McClelland RL, et al. Distribution of coronary artery calcium by race, gender, and

752 age: results from the Multi-Ethnic Study of Atherosclerosis (MESA). *Circulation*.  
753 2006;113(1):30-37.

754 48. Ma YC, et al. Modified glomerular filtration rate estimating equation for Chinese  
755 patients with chronic kidney disease. *J Am Soc Nephrol*. 2006;17(10):2937-2944.

756 49. Durlacher-Betzer K, et al. Interleukin-6 contributes to the increase in fibroblast  
757 growth factor 23 expression in acute and chronic kidney disease. *Kidney Int*.  
758 2018;94(2):315-325.

759 50. Gao C, et al. Microsomal Prostaglandin E Synthase-1-Derived PGE2 Inhibits  
760 Vascular Smooth Muscle Cell Calcification. *Arterioscler Thromb Vasc Biol*.  
761 2016;36(1):108-121.

762 51. Clinkenbeard EL, et al. Increased FGF23 protects against detrimental cardio-  
763 renal consequences during elevated blood phosphate in CKD. *JCI Insight*.  
764 2019;4(4).

765 52. Kukida M, et al. AT2 receptor stimulation inhibits phosphate-induced vascular  
766 calcification. *Kidney Int*. 2019;95(1):138-148.

767 53. Liu Y, et al. Apocynin Attenuates Cardiac Injury in Type 4 Cardiorenal Syndrome  
768 via Suppressing Cardiac Fibroblast Growth Factor-2 With Oxidative Stress  
769 Inhibition. *J Am Heart Assoc*. 2015;4(7).

770 54. Feng W, et al. Advanced oxidation protein products aggravate cardiac  
771 remodeling via cardiomyocyte apoptosis in chronic kidney disease. *Am J Physiol*  
772 *Heart Circ Physiol*. 2018;314(3):H475-H483.

773 55. Kong Y, et al. Statins ameliorate cholesterol-induced inflammation and improve  
774 AQP2 expression by inhibiting NLRP3 activation in the kidney. *Theranostics*.

775 2020;10(23):10415-10433.

776 56. Lovren F, et al. MicroRNA-145 targeted therapy reduces atherosclerosis.

777 *Circulation*. 2012;126(11 Suppl 1):S81-90.

778 57. Zhang F, et al. Long-term modifications of blood pressure in normotensive and

779 spontaneously hypertensive rats by gene delivery of rAAV-mediated cytochrome

780 P450 arachidonic acid hydroxylase. *Cell Res*. 2005;15(9):717-724.

781 58. Zang M, et al. Polyphenols stimulate AMP-activated protein kinase, lower lipids,

782 and inhibit accelerated atherosclerosis in diabetic LDL receptor-deficient mice.

783 *Diabetes*. 2006;55(8):2180-2191.

784 59. Hou G, et al. The discoidin domain receptor tyrosine kinase DDR1 in arterial

785 wound repair. *J Clin Invest*. 2001;107(6):727-735.

786 60. Zhang K, et al. Interleukin-18 Enhances Vascular Calcification and Osteogenic

787 Differentiation of Vascular Smooth Muscle Cells Through TRPM7 Activation.

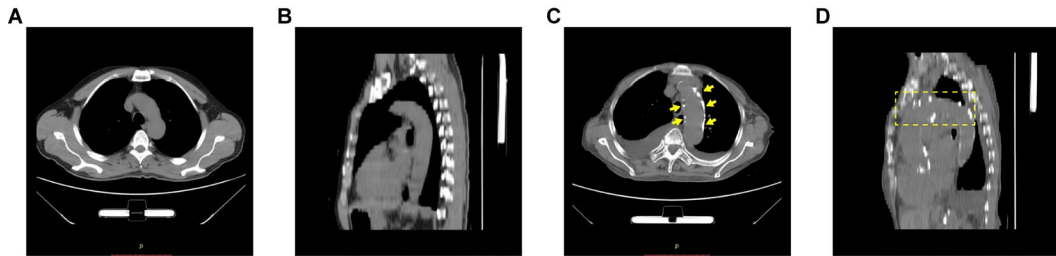
788 *Arterioscler Thromb Vasc Biol*. 2017;37(10):1933-1943.

789 61. Nass SA, et al. Universal Method for the Purification of Recombinant AAV

790 Vectors of Differing Serotypes. *Mol Ther Methods Clin Dev*. 2018;9:33-46.

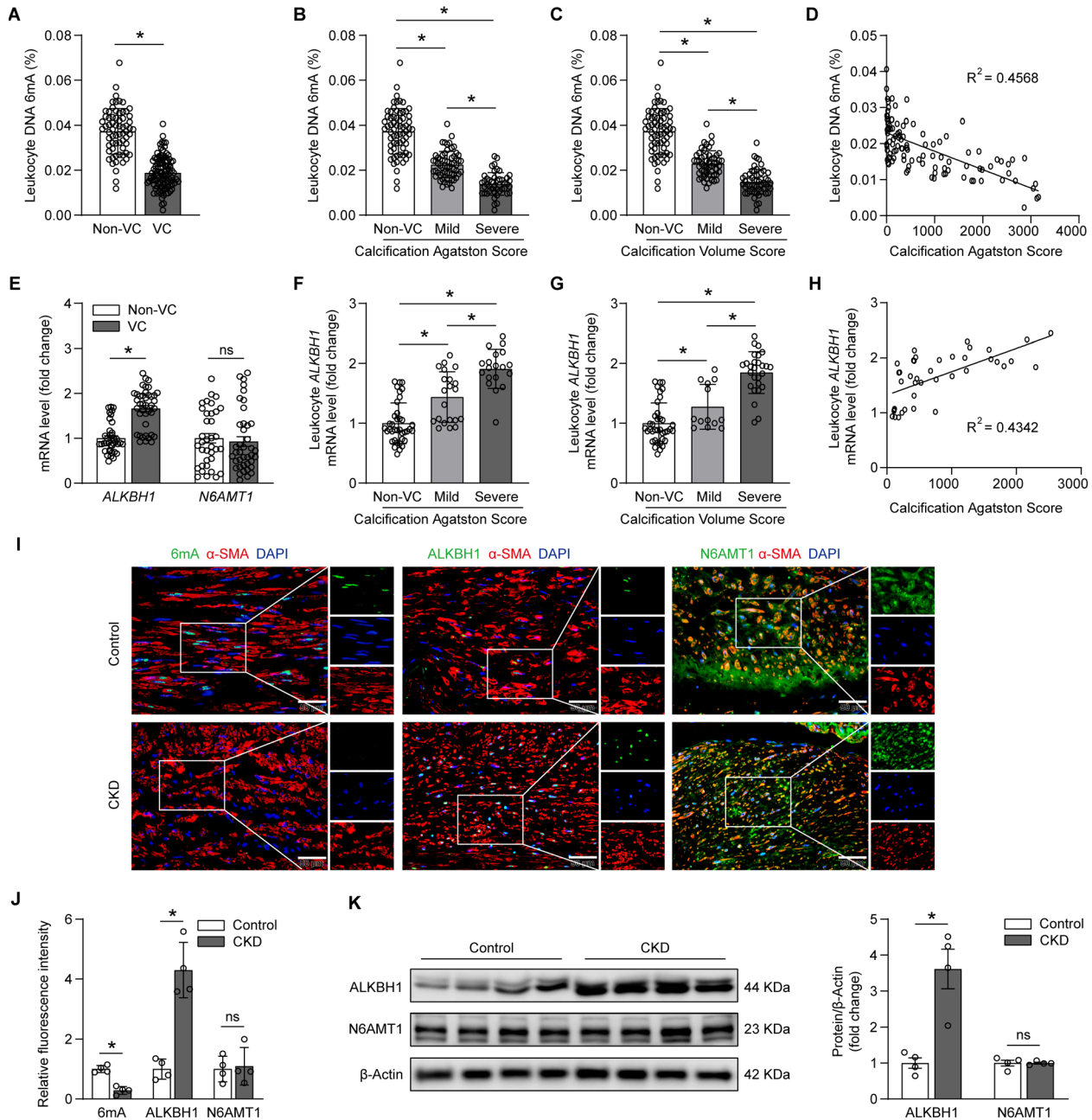
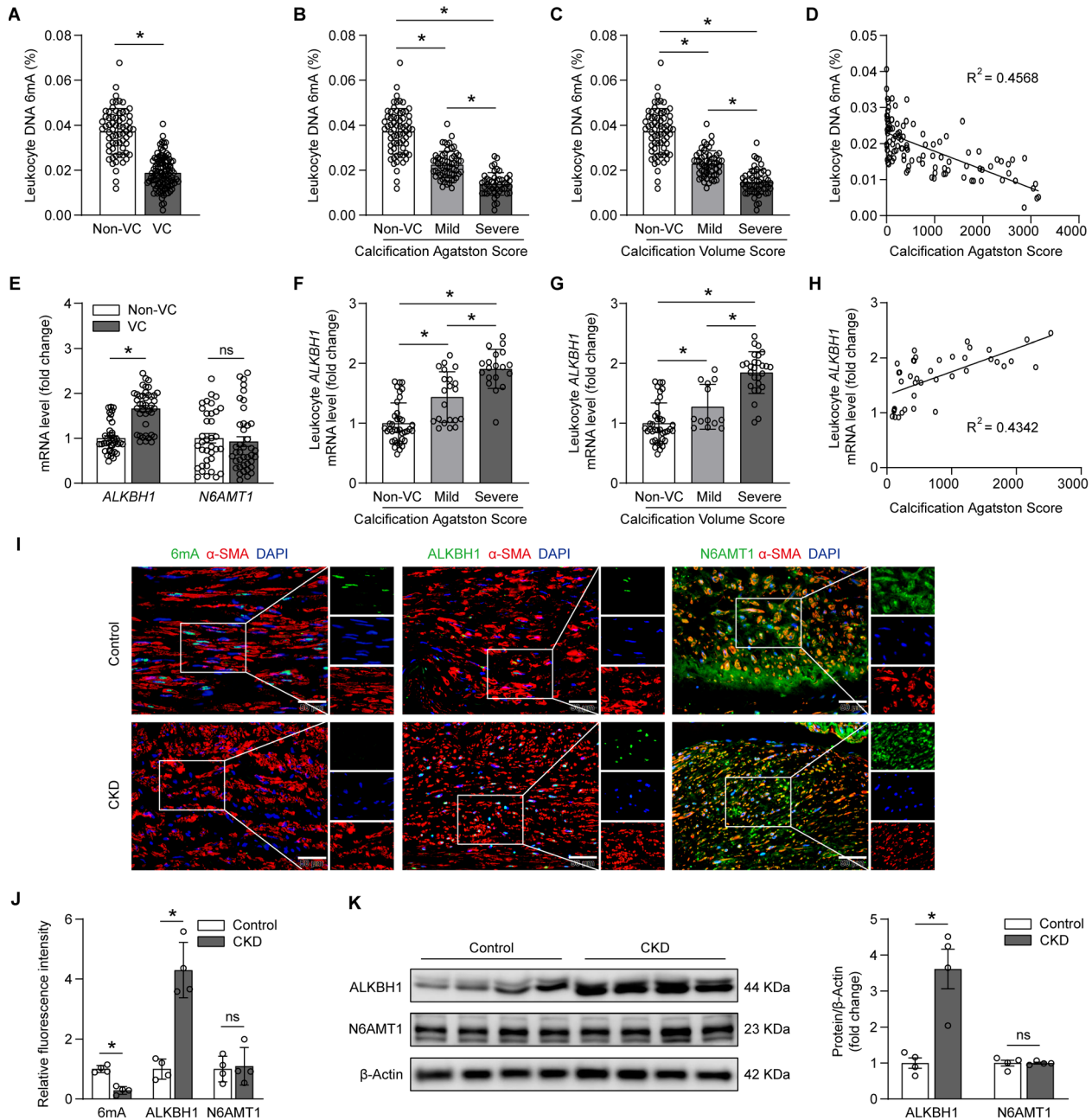
791

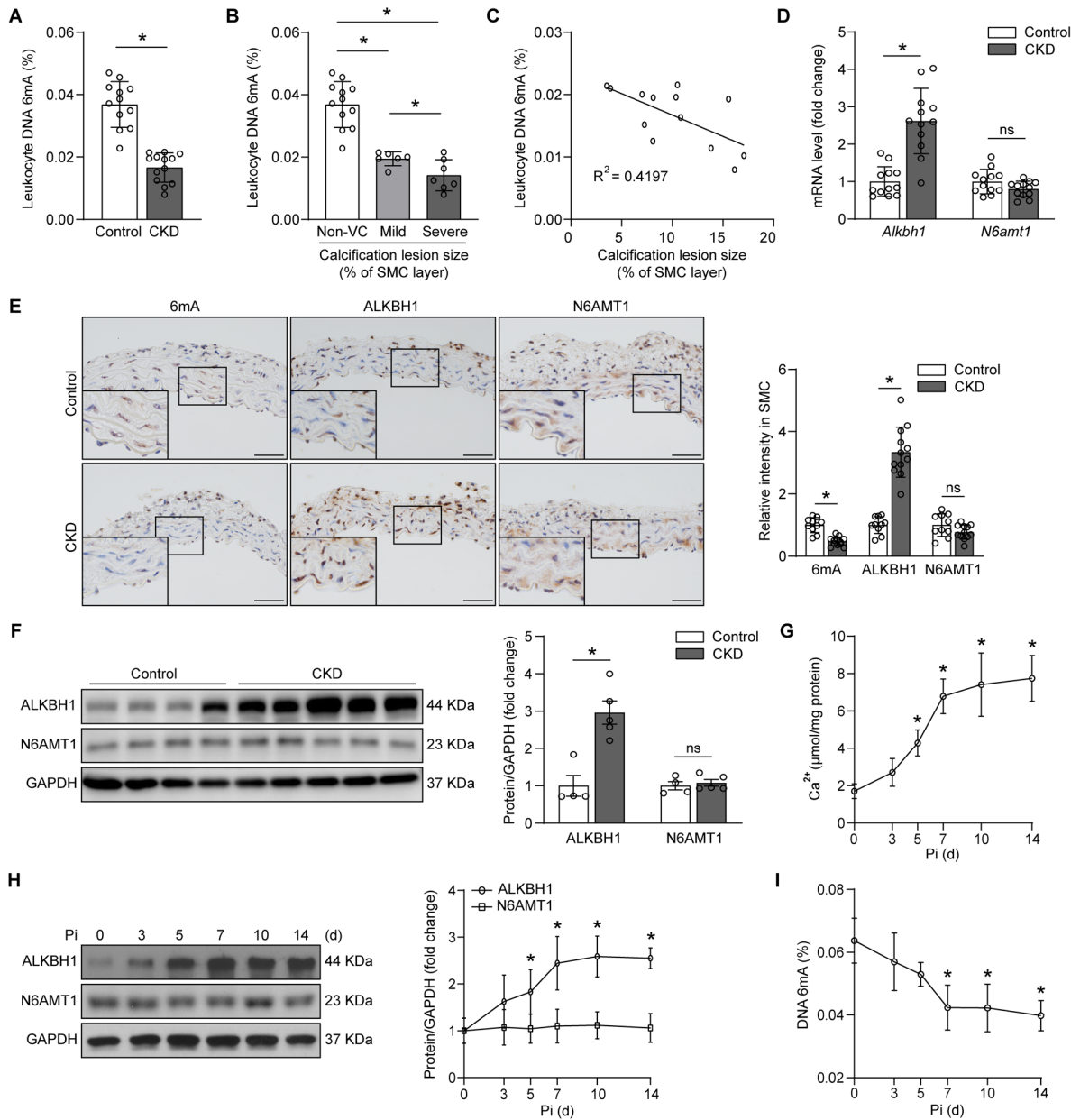
792 **Figures and figure legends**



794 **Figure 1. Representative images of multi-detector computed tomography (MDCT) scan of CKD patients with**  
795 **or without calcification. (A and B) Representative axial image (A) and sagittal reconstruction (B) of contrast-**  
796 **enhanced CT scan in CKD patients without calcification. (C and D) Representative axial image (C) and sagittal**  
797 **reconstruction (D) of contrast-enhanced CT scan showing aortic arch calcification in CKD patients.**

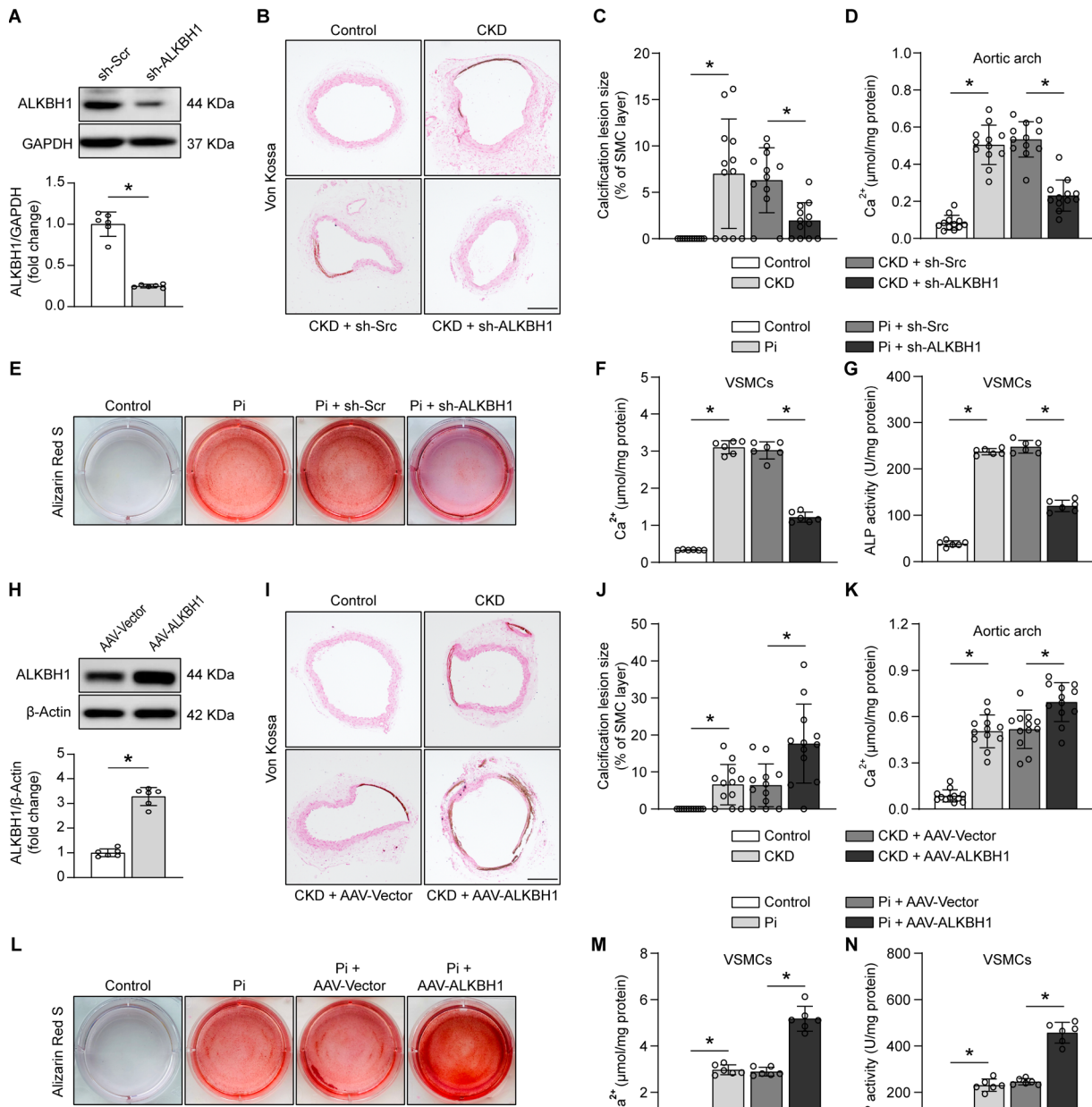
798





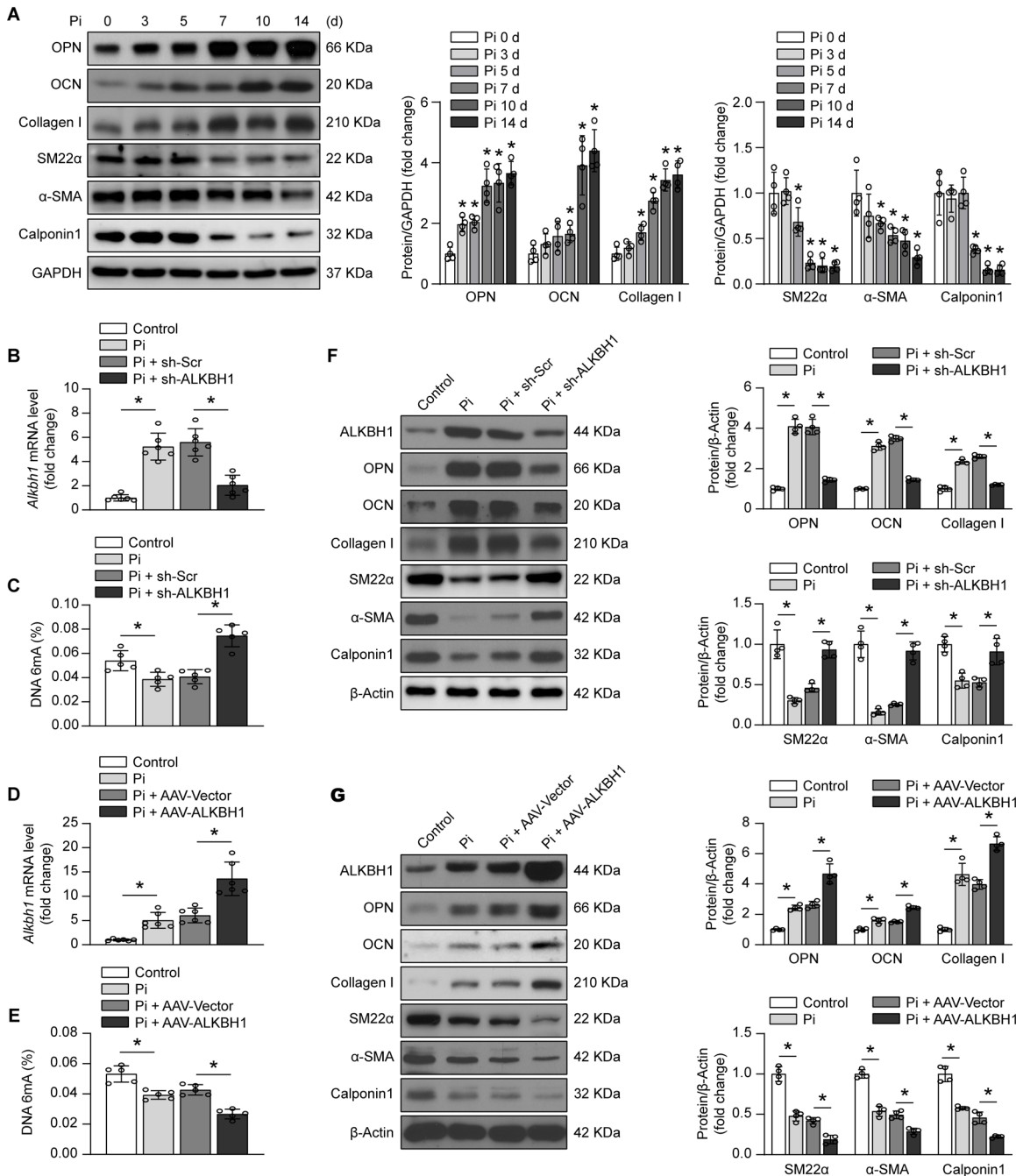
815

**Figure 3. ALKBH1-demethylated DNA 6mA modification is reduced in murine calcified arteries.** (A) Leukocyte DNA 6mA level in mice fed with adenine diet (CKD, n = 13) or normal chow diet (Control, n = 12) for 8 weeks. Leukocytes were isolated from peripheral blood. (B and C) Mice leukocyte DNA 6mA level in different subgroups defined by the percentage of calcification lesion size in aortic smooth muscle layer (B, n = 12 for Non-VC; n = 6 for Mild; n = 7 for Severe). Scatter dot plot of correlation between mice leukocyte DNA 6mA level and percentage of calcification lesion size in aortic smooth muscle layer from mice fed with adenine diet for 8 weeks (C, n = 13). (D) The mRNA expression levels of *Alkbh1* and *N6amt1* in leukocytes from mice with different diets (n = 12 per group). (E) Representative immunohistochemistry pictures and quantification of ALKBH1, N6AMT1, and 6mA in mice aortic smooth muscle layer (n = 10 for Control; n = 12 for CKD). Scale bars: 50 μm. (F) Western blot analysis of ALKBH1 and N6AMT1 expression in mice aortic arch (n = 4 for Control; n = 5 for CKD). (G-I) Calcium content (G), western blot analysis of ALKBH1 and N6AMT1 (H), and DNA 6mA level (I) in mice aortic rings incubated with osteogenic medium for the indicated time (0, 3, 5, 7, 10, and 14 days) (n = 4-6 per group). Statistical significance was assessed using two-tailed t-tests (A, and D-F), one-way ANOVA followed by Bonferroni test (B) or Dunnett's test (G-I), and Pearson's correlation coefficient analysis (C). All values are presented as means ± SD, ns: no significance, \*p < 0.05 vs. Pi (0 day) in G-I.



831  
832  
833  
834  
835  
836  
837  
838  
839  
840  
841  
842  
843  
844  
845  
846  
847

**Figure 4. ALKBH1 is essential for the regulation of vascular calcification.** (A) Western blot analysis identifying the ALKBH1 deficiency in arteries (n = 6 per group). Mice were injected via tail vein with AAV carrying scrambled shRNA (sh-Scr) or *Alkbh1* shRNA (sh-ALKBH1) at four weeks after adenine diet and then fed for another four weeks. (B-D) Von Kossa staining (B and C) and calcium content quantification of aortic arch (D) were performed in different experimental groups for detecting mineralization (n = 10-12 per group). Scale bar: 100 μm. (E) Photomicrographs of Alizarin red staining in mice primary VSMCs pre-transfected with indicated treatment and exposed in osteogenic medium for another 14 days (n = 6 per group). (F and G) Bar graphs representative of calcium content (F) and ALP activity (G) in mice primary VSMCs from all of the experimental cohorts (n = 6 per group). (H) ALKBH1 overexpression in arteries confirmed by western blot (n = 6 per group). Mice were injected with AAV-Vector or AAV-ALKBH1 at four weeks after the adenine diet and then fed for another four weeks. (I-K) Percentage of positive von Kossa staining (I and J) and calcium content (K) quantified in the aortic arch from the different cohorts (n = 10-12 per group). Scale bar: 100 μm. (L) Representative images of Alizarin red staining in mice primary VSMCs after indicated transfection and osteogenic medium exposure for another 14 days (n = 6 per group). (M and N) Scatter dot plots representative of calcium content (M) and ALP activity (N) in mice primary VSMCs from all of the experimental cohorts (n = 6 per group). Statistical significance was assessed using two-tailed t-tests (A and H) and one-way ANOVA followed by Dunnett's test (C-G, J-N). All values are presented as means ± SD, \*p < 0.05.



848

849 **Figure 5. ALKBH1 regulates VSMCs osteogenic reprogramming.** (A) Western blot analysis of osteogenic  
 850 phenotype marker (OPN, OCN, and Collagen I) and contractile phenotype marker (SM22α, α-SMA, and Calponin1)  
 851 expression in mice primary VSMCs cultured in osteogenic medium for 14 days. (B) Quantitative real time PCR  
 852 analysis of *Alkbh1* expression in mice primary VSMCs, which pre-transfected with AAV encoding scrambled or *Alkbh1*  
 853 shRNA for 48 hours, and then cultured in osteogenic medium for another 14 days. (C) Quantitative DNA 6mA level in  
 854 ALKBH1-deficient mice primary VSMCs. (D) Quantitative real time PCR analysis of *Alkbh1* expression in mice  
 855 primary VSMCs, which pre-infected with AAV-Vector or AAV-ALKBH1 for 48 hours, and then cultured in osteogenic  
 856 medium for another 14 days. (E) Quantitative DNA 6mA level in ALKBH1-overexpressed mice primary VSMCs. (F)  
 857 Western blot analysis of osteogenic phenotype marker and contractile phenotype marker expression in mice primary  
 858 VSMCs with ALKBH1 depletion. (G) Western blot analysis of osteogenic phenotype marker and contractile phenotype  
 859 marker expression in mice primary VSMCs with ALKBH1 overexpression. Statistical significance was assessed using  
 860 one-way ANOVA followed by Dunnett's test. n = 4-6 for each group. All values are presented as means  $\pm$  SD, \*p <  
 861 0.05 vs. Pi (0 day) in A.

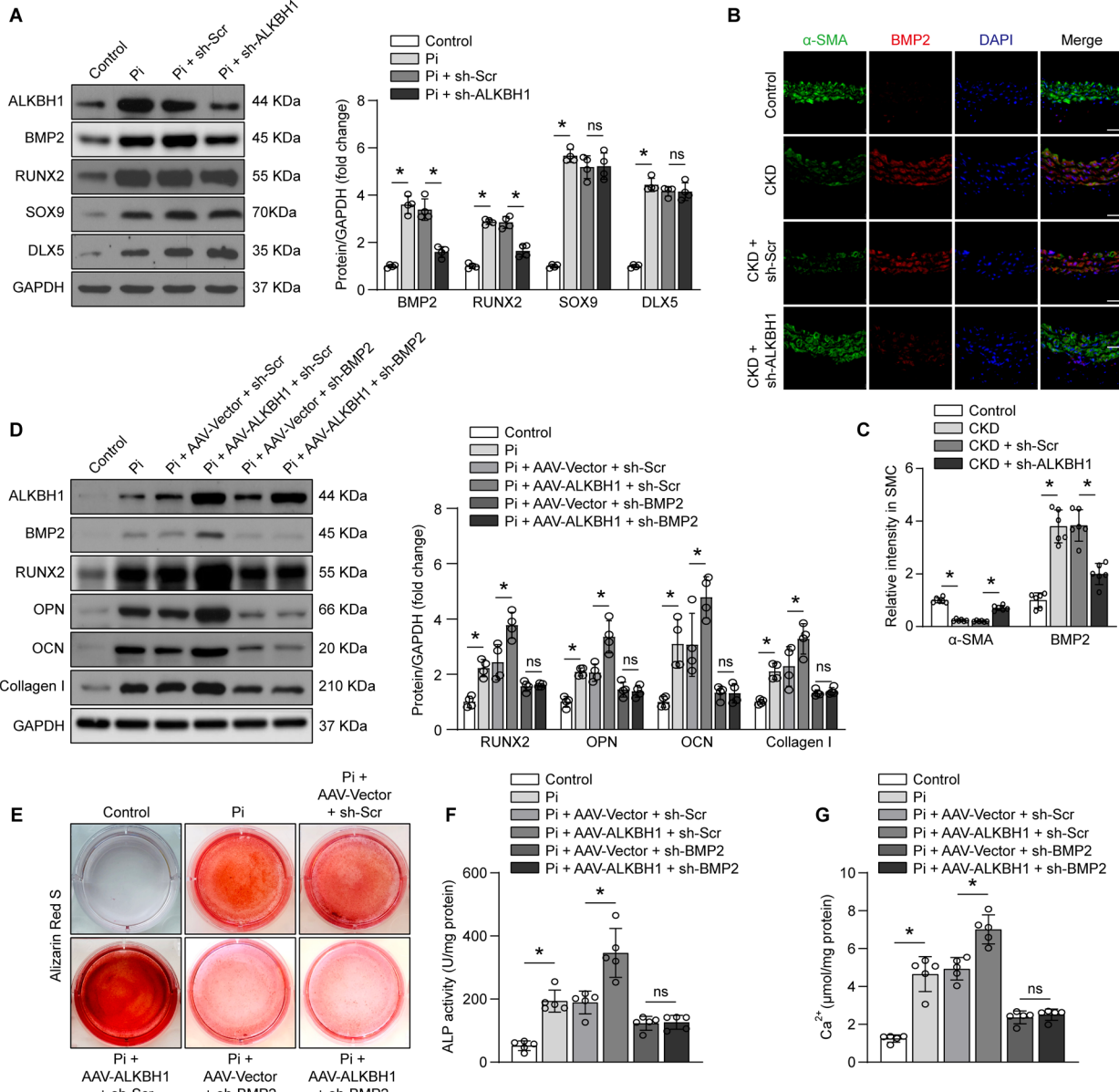
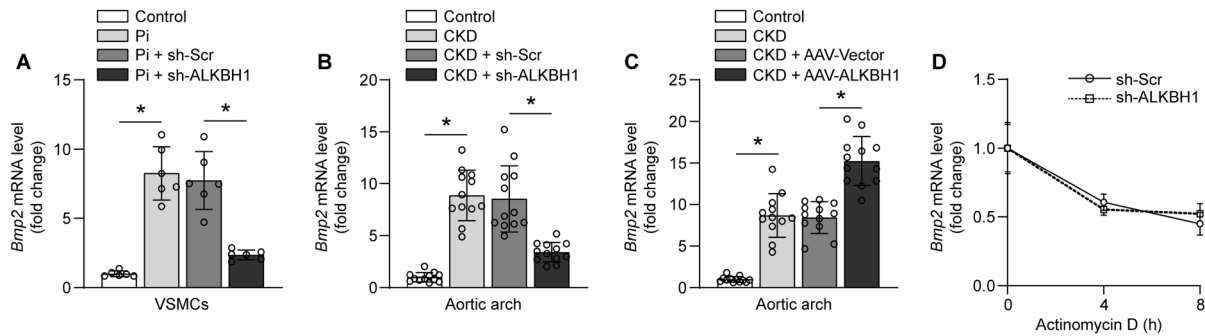


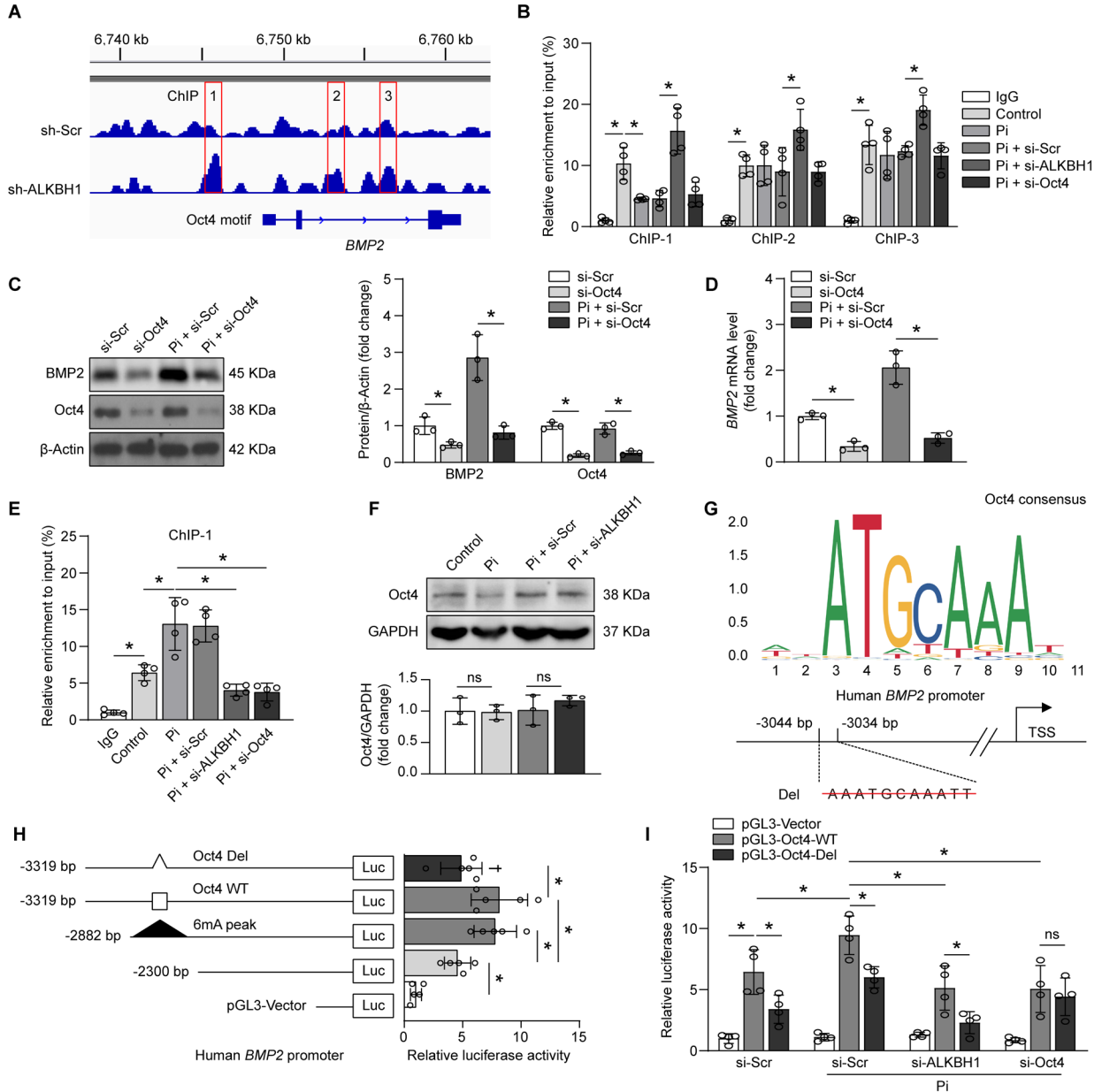
**Figure 6. BMP2 mediates the pro-calcifying effects of ALKBH1.** (A) Western blot analysis of ALKBH1, BMP2, RUNX2, SOX9, and DLX5 expression in calcified mice primary VSMCs with AAV sh-Scr or AAV sh-ALKBH1 transfection (n = 4 per group). (B and C) Representative immunofluorescence images (B) and quantification (C) of α-SMA and BMP2 co-stained in aortas from indicated experimental cohorts (n = 6 per group). Scale bar, 50 μm. (D) Western blot analysis of osteogenic phenotype marker (RUNX2, OPN, OCN, and Collagen I) expression in mice primary VSMCs, which pre-infected with AAV sh-Scr or AAV sh-BMP2 together with AAV-Vector or AAV-ALKBH1 and then incubated in calcifying medium for another 14 days. (E and F) Alizarin red staining (E) and ALP activity assay (F) performed in all of the groups for detecting calcification formation (n = 4-5 per group). (G) Quantification of calcium content in mice aortic ring cultured in calcifying medium with indicated transfection (n = 5 per group). Statistical significance was assessed using one-way ANOVA followed by Dunnett's test (A-C) or Bonferroni test (D-G). All values are presented as means ± SD, ns: no significance, \*p < 0.05.



874

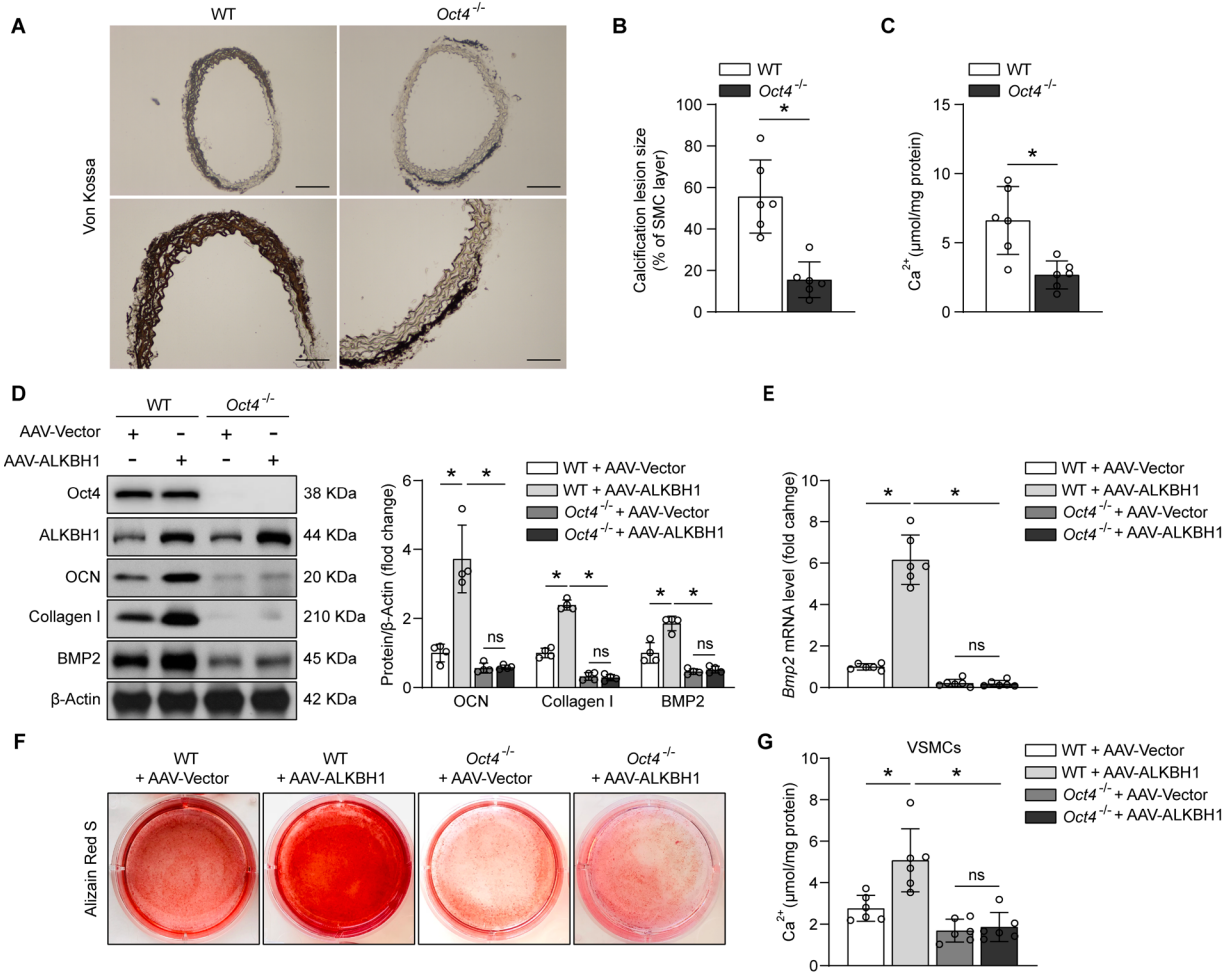
875 **Figure 7. BMP2 is regulated by ALKBH1 in transcriptional level.** (A) Quantitative real time PCR analysis of *Bmp2*  
 876 expression in primary mice VSMCs with ALKBH1 depletion (n = 6 per group). (B and C) Quantitative real time PCR  
 877 analysis of *Bmp2* expression in the aortic arch from mice with ALKBH1 knockdown (B) or ALKBH1 overexpression (C)  
 878 (n = 12 per group). (D) Quantitative real time PCR analysis of *Bmp2* expression in mice primary VSMCs treated with  
 879 actinomycin D (5 mg/mL) for a different time after AAV sh-Scr or AAV sh-ALKBH1 transfection (n = 3 per group).  
 880 Gene expression was normalized to *Gapdh*. Statistical significance was assessed using one-way ANOVA followed by  
 881 Dunnett's test. All values are presented as means  $\pm$  SD, \*p < 0.05.

882



883

884 **Figure 8. ALKBH1-dependent 6mA demethylation promotes Oct4 binding to the BMP2 promoter and activates**  
 885 **BMP2 transcription.** (A) Integrative genomics viewer plots showing the increasing 6mA peaks (selected one marked  
 886 as ChIP1-3) in human BMP2 gene (hg19) region with ALKBH1 knockdown via shRNA lentiviral constructs. (B) ChIP-  
 887 qPCR assay displaying the 6mA enrichment on the three BMP2 fragments in treated HASMCs ( $n = 4$  per group). (C)  
 888 and (D) Quantitative western blot (C) and real time PCR analysis of BMP2 expression (D) in HASMCs with scramble  
 889 or OCT4 siRNA transfection under calcifying condition ( $n = 3$  per group). (E) ChIP-qPCR assay with Oct4 or IgG  
 890 antibody for the ChIP-1 enrichment in treated HASMCs ( $n = 4$  per group). (F) Western blot analysis of Oct4 in  
 891 HASMCs incubated with osteogenic medium after transfection with scrambled siRNA (si-Scr) or ALKBH1 siRNA (si-  
 892 ALKBH1). (G) Logos of the standard Oct4 motif and schematic of human BMP2 promoter showing wide-type (WT)  
 893 and deleted (Del) binding sites for Oct4 within the first 6mA peak. (H) Bar graphs representative of the luciferase  
 894 activity analyzed in HASMCs after co-transfection with control Renilla luciferase plasmid and serial deletion  
 895 constructs of BMP2 promoter-driven luciferase reporters containing WT or Del Oct4 site ( $n = 5$  per group). (I) Relative  
 896 promoter activities measured by dual-luciferase reporter assay in HASMCs, which pre-treated with indicated siRNA  
 897 and then infected with pGL3-Oct4-WT or pGL3-Oct4-Del under calcifying condition ( $n = 4$  per group). Statistical  
 898 significance was assessed using one-way ANOVA followed by Bonferroni test. All values are presented as means  $\pm$   
 899 SD, ns: no significance, \* $p < 0.05$ .



901 **Figure 9. Oct4 mediates the regulation of ALKBH1 on BMP2.** (A-C) Representative von Kossa staining images (A)  
902 and quantification (B) of aortic rings from *Oct4*<sup>WT/WT</sup>-Myh11-Cre/ERT2 (WT) and *Oct4*<sup>F/F</sup>-Myh11-Cre/ERT2 (*Oct4*<sup>-/-</sup>)  
903 mice cultured in osteogenic medium for 14 days. Bar graphs representative of calcium content (C) from these two  
904 groups (n = 6 per group). Scale bar: 100 µm. (D-G) Western blot analysis (D) of BMP2, Oct4, ALKBH1, and  
905 osteogenic phenotype marker (OCN and Collagen I) expression in calcified primary VSMCs from WT or *Oct4*<sup>-/-</sup> mice  
906 transfected with AAV-Vector or AAV-ALKBH1. Quantitative real time PCR analysis of *Bmp2* expression in all of the  
907 experimental cohorts (E). Alizarin red staining (F) and calcium content quantification (G) performed in all of the  
908 groups for detecting calcification formation (n = 4-6 per group). Statistical significance was assessed using two-tailed  
909 t-tests (B and C) and one-way ANOVA followed by Bonferroni test (D-G). All values are presented as means ± SD, ns:  
910 no significance, \*p < 0.05.

911 **Table and table legend**912 **Table 1.** Basal characteristics in CKD patients with or without calcification.

Characteristics	Non-VC (n = 67)	VC (n = 106)	P value
<b>Demographic characteristics</b>			
Male (%)	46 (68.7)	64 (60.4)	0.27
Age (year)	59.6±14.9	64.7±13.2	<b>0.02</b>
BMI (kg/m <sup>2</sup> )	23.4 (21.7-26.0)	23.2 (20.1-25.8)	0.149
SBP (mmHg)	135.8±23.4	145.6±20.8	<b>0.005</b>
DBP (mmHg)	86 (75-93)	80 (74-86)	<b>0.011</b>
<b>Plasma biochemical characteristics</b>			
K (mmol/L)	4.14±0.62	4.39±0.67	<b>0.014</b>
Ca (mmol/L)	2.15 (2.04-2.24)	2.17 (2.07-2.27)	0.218
Pi (mmol/L)	1.29 (0.97-1.70)	1.31 (1.07-1.66)	0.286
GLU (mmol/L)	5.04 (4.37-5.98)	5.42 (4.51-7.69)	0.17
BUN (mmol/L)	10.42 (5.18-21.26)	16.36 (10.37-22.62)	<b>0.013</b>
CREA (μmol/L)	387.9 (91.3-936.5)	500.1 (249.5-985.8)	0.126
suPAR (pg/mL)	4146 (2692-5432)	4809 (3555-6420)	0.0668
eGFR (mL/min·per 1.73m <sup>2</sup> )	14.78 (5.18-73.78)	8.56 (4.71-18.81)	0.072
URCA (μmol/L)	399 (322-501)	384 (298-464)	0.254
ALB (g/L)	37.26±5.87	34.92±5.43	<b>0.008</b>
ALT (U/L)	14 (8-26)	11 (6-15)	<b>0.009</b>
AST (U/L)	16 (12-21)	14 (12-18)	0.682
ALP (U/L)	64 (49-75)	77 (60-107)	<b>&lt;0.001</b>
CHOL (mmol/L)	3.95 (3.58-4.79)	4.10 (3.17-4.80)	0.516
TG (mmol/L)	1.75 (1.04-2.47)	1.24 (0.91-1.81)	0.114
HDL-C (mmol/L)	1.11 (0.84-1.36)	1.05 (0.79-1.44)	0.684
LDL-C (mmol/L)	2.28 (1.98-3.12)	2.41 (1.61-3.29)	0.503

913 Values are expressed as mean ± SD or median (25th-75th quartiles) for continuous variables and n (%) for  
 914 categorical variables, respectively. Statistical significance was assessed using Student's t-test (all characteristics  
 915 except gender) or nonparametric Mann-Whitney test (gender). BMI, body mass index; SBP, systolic blood pressure;  
 916 DBP, diastolic blood pressure; K, potassium; Ca, calcium; Pi, phosphate; GLU, glucose; BUN, blood urea nitrogen;  
 917 CREA, creatinine; suPAR, soluble urokinase plasminogen activator receptor; eGFR, estimated glomerular filtration  
 918 rate; URCA, uric acid; ALB, albumin; ALT, alanine transaminase; AST, aspartate aminotransferase; ALP, alkaline  
 919 phosphatase; CHOL, total cholesterol; TG, triglyceride; HDL-C, high-density lipoprotein cholesterol; LDL-C, low-  
 920 density lipoprotein cholesterol.